# New PI(4,5)P$_2$- and membrane proximal integrin–binding motifs in the talin head control β3-integrin clustering

Frédéric Saltel,[1] Eva Mortier,[2] Vesa P. Hytönen,[3] Marie-Claude Jacquier,[1] Pascale Zimmermann,[2] Viola Vogel,[3] Wei Liu,[4] and Bernhard Wehrle-Haller[1]

[1]Department of Cellular Physiology and Metabolism, University Medical Center, University of Geneva, 1211 Geneva 4, Switzerland
[2]Laboratory for Signal Integration in Cell Fate Decision, Department of Human Genetics, Catholic University Leuven, B-3000 Leuven, Belgium
[3]Department of Materials, Swiss Federal Institute of Technology Zürich, CH-8093 Zürich, Switzerland
[4]Department of Biosciences and Nutrition, Karolinska Institute, 141 57 Huddinge, Sweden

Integrin-dependent adhesion sites consist of clustered integrins that transmit mechanical forces and provide signaling required for cell survival and morphogenesis. Despite their importance, the regulation of integrin clustering by the cytoplasmic adapter protein talin (Tal) and phosphatidylinositol (PI)-4,5-biphosphate (PI(4,5)P$_2$) lipids nor their dynamic coupling to the actin cytoskeleton is fully understood. By using a Tal-dependent integrin clustering assay in intact cells, we identified a PI(4,5)P$_2$-binding basic ridge spanning across the F2 and F3 domains of the Tal head that regulates integrin clustering. Clustering requires a new PI(4,5)P$_2$-binding site in F2 and is negatively regulated by autoinhibitory interactions between F3 and the Tal rod (Tal-R). The release of the Tal-R exposes a new β3-integrin–binding site in F3, enabling interaction with a membrane proximal acidic motif, which involves the formation of salt bridges between K$^{316}$ and K$^{324}$ with E$^{726}$ and D$^{723}$, respectively. This interaction shields the β-integrin tail from reassociation with its α subunit, thereby maintaining the integrin in a substrate-binding and clustering-competent form.

## Introduction

Integrins are heterodimeric transmembrane receptors consisting of an α and β subunit that are crucial for cell adhesion and migration during development as well as for tissue homeostasis in the adult organism (Hynes, 2002). Integrins form the core of a biological system that converts mechanical information such as adhesion strength and sheer forces into chemical signals inducing multiple cellular functions such as mobility, proliferation, and survival. This relay function is directly linked to the ability of integrins to form clusters in the membrane and to mechanically connect to the cytoskeleton via specific adapter proteins.

Integrin clustering manifests itself in different biological structures such as in force-bearing focal adhesions of fibroblasts in adhesive and tightly sealing podosome belts of osteoclasts or in the signaling platform created by the immunological synapse (Geiger and Bershadsky, 2001; Dustin and Colman, 2002; Chabadel et al., 2007). However, despite the physiological importance, neither the mechanisms and protein–protein interactions leading to integrin clustering nor the subsequent creation of chemical signals is well understood.

In adherent cells, integrin clustering occurs in response to binding to immobilized ligands and unclasping of its transmembrane and cytoplasmic domains (Cluzel et al., 2005). In suspended cells, the binding of soluble ligands to integrin receptors requires the cytoplasmic adapter proteins kindlin and talin (Tal), both of which are also essential for integrin-dependent

Correspondence to Bernhard Wehrle-Haller: Bernhard.Wehrle-Haller@unige.ch

F. Saltel's present address is European Institute of Chemistry and Biology (U889), University of Bordeaux I and 2, 33607 Pessac, France.

V.P. Hytönen's present address is Institute of Medical Technology, University of Tampere, 33520 Tampere, Finland.

Abbreviations used in this paper: FERM, band F.1–ezrin-radixin-merlin; FL, full length; MD, molecular dynamics; MP, membrane proximal; NMR, nuclear magnetic resonance; PC, phosphatidylcholine; PE, phosphatidylethanolamine; PI, phosphatidylinositol; PI(4,5)P$_2$, PI-4,5-biphosphate; PS, phosphatidylserine; SPR, surface plasmon resonance; Tal, talin; Tal-H, Tal head; Tal-R, Tal rod; TIRF, total internal reflection fluorescence.
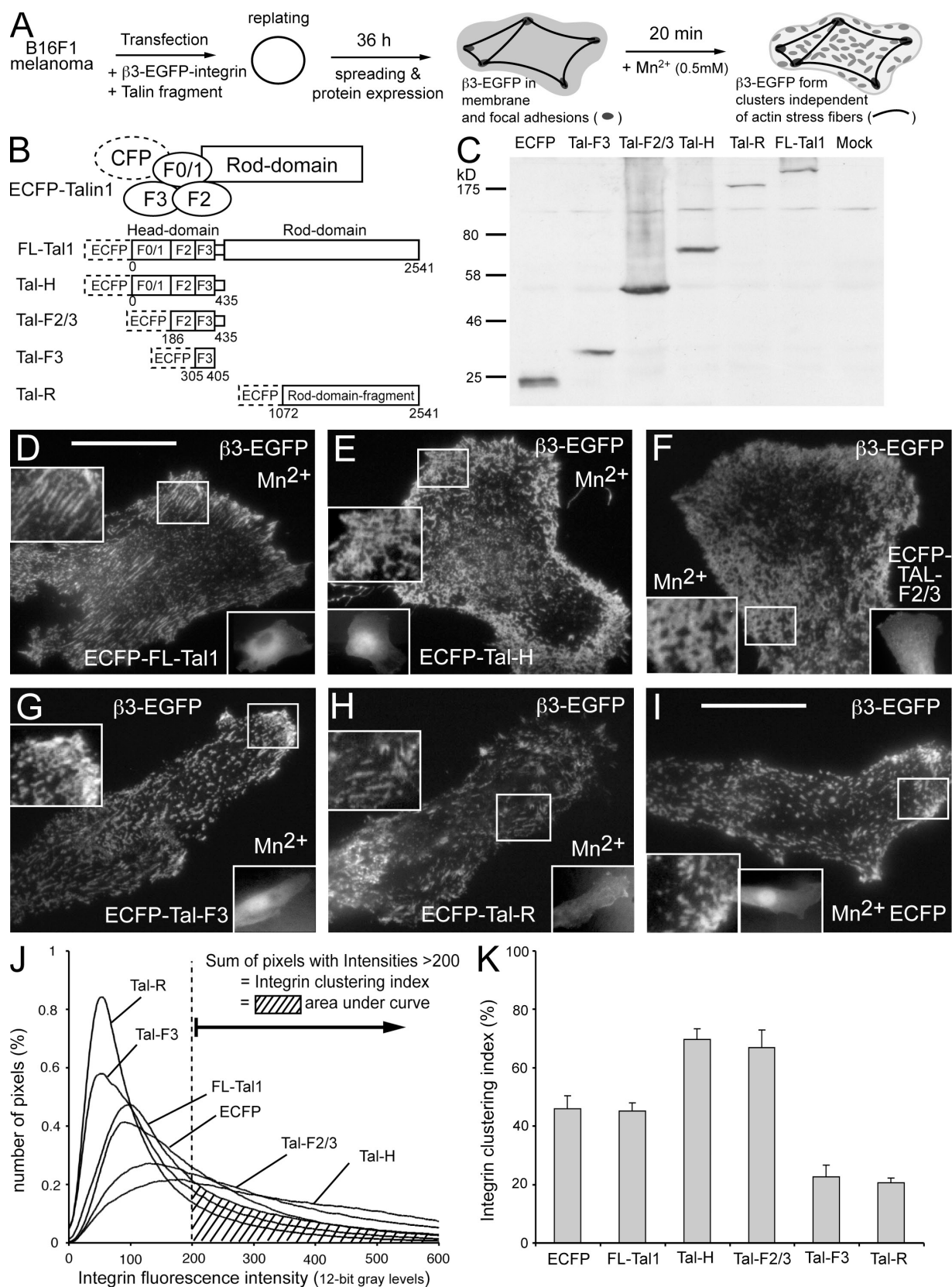
Figure 1. **The F2 and F3 domains of Tal-H are required for β3-integrin clustering.** (A and B) Scheme of the Tal-dependent β3-integrin clustering protocol (A) and ECFP-tagged Tal fragments (B). (C) Western blot with anti-EGFP antibodies of equivalent amounts of cell lysates (50% for ECFP) of transiently transfected B16F1 cells. (D–I) Representative TIRF images (EGFP channel) of $Mn^{2+}$-stimulated B16F1 cells plated on serum-coated coverslips and double transfected with β3-EGFP-integrin (D–I) and ECFP–FL-Tal (D), ECFP–Tal-H (E), ECFP–Tal-F2/3 (F), ECFP–Tal-F3 (G), ECFP-tagged Tal-R (H), and ECFP only (I). Magnified views of the boxed areas and ECFP epifluorescence are shown in the insets. (J) Averaged (n > 25) fluorescence intensity histograms of β3-EGFP-integrin

adhesion and spreading of platelets (Petrich et al., 2007b; Ma et al., 2008; Moser et al., 2008; Zhang et al., 2008). The conformational changes of integrins in response to ligand binding and tail unclasping have been termed integrin activation, which has been monitored by electron microscopy, gel filtration chromatography, and conformation-specific antibodies (Xiong et al., 2001, 2002; Takagi et al., 2002; Kim et al., 2003; Xiao et al., 2004). Integrin activation can be induced by the expression of Tal head (Tal-H), which requires $R^{358}$ and a basic loop in the F3 subdomain that bind to a conserved Tyr (NPLY) and membrane proximal (MP) aromatic motif in the cytoplasmic tail of the β-integrin subunit, respectively (Tadokoro et al., 2003; Wegener et al., 2007). In turn, premature integrin activation, for example, of the platelet receptor αIIbβ3 is prevented by transmembrane domain association at the interface between the plasma membrane and the cytoplasm, which is mediated by aromatic ($GFFKR^{995}$) and electrostatic interactions ($D^{723}$; $R^{995}$; Hughes et al., 1996; Kim et al., 2009; Lau et al., 2009; Zhu et al., 2009). In adherent cells, the release of this autoinhibitory interaction, for example, by the mutation of one of the charged residues (D723A), $Mn^{2+}$-induced integrin activation in the ectodomain, or the overexpression of Tal-H each result in ligand-dependent integrin clustering that occurs even in the absence of a functional actin cytoskeleton (Kim et al., 2004; Cluzel et al., 2005). Although Tal-H is sufficient for β3-integrin clustering (Cluzel et al., 2005) and to stabilize integrin-dependent cell spreading (Zhang et al., 2008), full-length (FL) Tal (FL-Tal) is required to connect integrins to stress fibers, which enables cell contractility–mediated mechanosensing (Zhang et al., 2008).

Although, the activation and clustering of integrins requires Tal-H, the reverse does not hold: Tal is not recruited to antibody-clustered low-affinity integrins unless the binding of small soluble ligands induces the high-affinity conformation (Miyamoto et al., 1995). Furthermore, in *Drosophila melanogaster*, mutation of the residue analogous to $R^{358}$ in mammalian Tal, which disrupts integrin activation, induces only a mild muscle attachment defect, which is compensated by the expression of an activated integrin α subunit (Tanentzapf and Brown, 2006). This reveals an apparent contradiction between the role of Tal for integrin activation and its recruitment to clustered integrins, raising several questions regarding the access of Tal to the cytoplasmic tail of integrins and how this interaction is controlled, for example, by phosphatidylinositol (PI)-4,5-biphosphate ($PI(4,5)P_2$)–induced Tal activation (Martel et al., 2001; Yan et al., 2001; Goksoy et al., 2008).

Furthermore, because the details of the interplay between mechanosensing and biochemical signaling required for the Tal-dependent maturation of cell adhesions remain unknown (Vogel and Sheetz, 2009), it is especially critical to design experiments that dissect the mechanisms of Tal-dependent integrin clustering from its role in force-induced maturation of cell substrate adhesions. In this study, we describe an experimental

system that allows quantification and molecular analysis of diffusion-controlled interactions between integrin and Tal, resulting in integrin clustering in the absence of force. By quantifying the clustering behavior of $Mn^{2+}$-activated integrins in the presence of FL-Tal, Tal-H, Tal rod (Tal-R), and various Tal mutants, we identified $PI(4,5)P_2$- and integrin-binding motifs in Tal-H critical for integrin clustering. Our data support a role for $PI(4,5)P_2$-induced Tal-R dissociation from Tal-H and simultaneous tethering of Tal-H to $PI(4,5)P_2$-enriched membranes, hereby exposing a hidden MP integrin binding interface, which is critically required for integrin clustering.

## Results

### Characterization of the integrin-clustering activity in Tal

In adherent, contractile cells, the rapid formation and force-dependent maturation of integrin clusters into focal adhesions prevent the detailed analysis of adapter protein interactions with extracellular matrix–bound integrins in living cells (Zaidel-Bar et al., 2003). To dissect the mechanisms leading to diffusion-driven Tal association with ligand-bound integrins and the resulting formation of integrin clusters, we developed an experimental system in which the clustering of β3-integrins can be reversibly induced in adherent B16F1 melanoma cells. De novo clusters of EGFP-tagged β3-integrins can be induced within 10 min by the addition of 0.5 mM $Mn^{2+}$ to the medium, resulting in the recruitment of endogenous Tal, independent of a linkage to F-actin or focal adhesion adapters such as vinculin or paxillin (Cluzel et al., 2005). Consistent with an immature focal adhesion state, F-actin–independent, $Mn^{2+}$-induced integrin clusters disappeared within 5–10 min after $Mn^{2+}$ washout (not depicted) but were strictly dependent on surface-bound αvβ3-integrin ligands such as vitronectin, fibronectin, or serum and were not formed on laminin (Fig. S1). When measured by FRAP, $Mn^{2+}$ treatment did not alter integrin dynamics in actin-associated focal adhesions (Cluzel et al., 2005), suggesting that $Mn^{2+}$ treatment reduces the energy threshold for integrin-unfolding (activation; Xiao et al., 2004) without affecting the dynamic association with intracellular adapter proteins or their extracellular ligands. Therefore, this inducible integrin activation system can be used to analyze diffusion-controlled Tal-mediated integrin clustering in living cells, independent of the mechanical aspects of focal adhesion maturation.

### Integrin clustering requires both the F2 and F3 subdomains of the Tal-H

To determine the role of the different Tal domains for integrin clustering, we coexpressed ECFP-tagged FL or truncated Tal1 fragments with wild-type β3-EGFP-integrin in B16F1 melanoma cells and stimulated them with $Mn^{2+}$ (Fig. 1 B). After 20 min, cells were fixed, and the β3-integrin clustering index

transfected cells as shown in D–I. The dashed line represents the fluorescence intensity threshold (>200 12-bit gray levels) that was used to calculate the integrin clustering index (K). Histograms are from one representative experiment, whereas the integrin clustering index (K) is the mean of $n > 3$ (SEM) experiments. Bars: (D and E) 25 µm; (F–I) 20 µm.

was determined from images of the cell to substrate interface obtained by total internal reflection fluorescence (TIRF) microscopy. Cells exhibiting a majority of pixels with weak fluorescence intensity (nonclustered integrins) showed a low clustering index. In contrast, $Mn^{2+}$-induced integrin clustering increased the number of high-intensity pixels at the expense of low-intensity pixels, resulting in an increase in the clustering index (Fig. 1, J and K). Transient transfection of wild-type β3-EGFP-integrin increased surface expression over endogenous integrin by 4.65 ± 0.55–fold, as measured by FACS using a hamster anti–mouse β3-integrin mAb (see Fig. 5 J). In comparison, the expression levels of FL-Tal were twice that of endogenous Tal (Fig. 2, A and B), which was similar to that of the different Tal fragments (Fig. 1 C).

Despite an increase in expression, FL-Tal did not alter the degree of $Mn^{2+}$-induced integrin clustering when compared with ECFP-transfected control cells (Fig. 1, D, I, and K). However, the expression of Tal-H or Tal-F2/3 fragments increased $Mn^{2+}$-induced integrin clustering (Fig. 1, E and F). In contrast, the integrin-binding Tal-F3 domain decreased integrin clustering compared with control levels (Fig. 1, G and K). Similarly, the expression of a Tal-R fragment containing the F-actin–binding site, several vinculins, and the second integrin-binding site decreased integrin clustering (Fig. 1, H and K).

To correlate β3-EGFP-integrin clustering with Tal localization, we expressed mCherry-tagged FL-Tal, Tal-H, and Tal-R. A perfect overlap between integrin clusters and FL-Tal was detected (Fig. S2 A). In contrast, mCherry–Tal-H colocalized with β3-EGFP-integrin clusters in the cell center and periphery but was excluded from high-intensity β3-integrin clusters in the periphery (Fig. S2 B). However, mCherry–Tal-R accumulated in peripheral high-intensity β3-integrin clusters while being excluded from central integrin clusters (Fig. S2 C). As actomyosin-dependent contraction is responsible for the higher density of β3-EGFP-integrin in peripheral focal adhesions (Ballestrem et al., 2001), Tal-H appears to be excluded, whereas Tal-R is attracted to force-bearing focal adhesion sites.

Consistent with the absence of Tal-H association with F-actin, the F-actin network appears to be deconnected from Tal-H–dependent integrin clusters (Fig. S3), suggesting the absence of mechanical coupling to the actin cytoskeleton. Moreover, in cells coexpressing Tal-H and Tal-R, the latter demonstrated a vinculin-like distribution at streaklike peripheral adhesions, being excluded from the surrounding Tal-H–induced network of clustered integrins (Fig. S3). These data suggest a critical role of Tal-R to recruit FL-Tal to F-actin–vinculin-containing focal adhesions, whereas the Tal-F2/3 domain is responsible for integrin clustering.

### Tal activation is a prerequisite for integrin clustering

The failure of overexpressed FL-Tal to increase integrin clustering above levels reached with endogenous Tal suggested that Tal activation and not its cytoplasmic concentration was limiting the degree of integrin clustering. To release the proposed intramolecular inhibitory interaction between Tal-R and Tal-F3 (Goksoy et al., 2008; Goult et al., 2009), we introduced an activating mutation into the basic $K^{318}$–$K^{324}$ loop in Tal-F3 (K318A) and expressed it within the context of FL-Tal. In response to $Mn^{2+}$, the K318A FL-Tal mutant augmented integrin clustering, although only to ∼50% when compared with that induced by Tal-H (Fig. 2 D). Importantly, when introduced into Tal-H, the K318A as well as the similarly behaving K318A/K320A mutant did not affect integrin clustering (see Fig. 4). This suggests that the partial increase in clustering of the K318A FL-Tal mutant results from partial Tal activation. This notion is consistent with the large binding interface between the Tal-F3 and Tal-R domain, as proposed by Goult et al. (2009), making it difficult to completely eliminate Tal autoinhibition by the K318A FL-Tal mutant.

### The Tal-F2 and Tal-F3 domains contain PI(4,5)P$_2$-binding sites

Because the release of the intramolecular interaction between Tal-R and Tal-H correlated with increased integrin clustering, we wanted to further investigate Tal-H interaction with PI(4,5)P$_2$, which is a known activator of Tal. In addition to Tal (Martel et al., 2001; Goksoy et al., 2008), the activation of the band F.1–ezrin-radixin-merlin (FERM) domain–containing proteins radixin and ezrin is also controlled by PI(4,5)P$_2$ binding (Barret et al., 2000; Hamada et al., 2000; Fievet et al., 2004). Therefore, we decided to identify possible PI(4,5)P$_2$-binding sites in Tal-H by examining the surface of Tal-F2/3 for clusters of basic amino acids (Fig. 3 A). When compared with radixin or ezrin, Tal was missing the PI(4,5)P$_2$-binding motif previously identified in these proteins (Barret et al., 2000; Hamada et al., 2000). Instead, Tal-H exhibited clusters of basic amino acids not present in these FERM domain proteins. For example, in Tal-F2, the shortening of α-helix 3 exposed a patch of three basic amino acids (Fig. 3 B). In Tal-F3, the long loop between β-sheets 1 and 2 created a basic finger, which was significantly shorter in other FERM domain proteins (Fig. 3 C) and is proposed to be involved in Tal-R binding (Goult et al., 2009).

To test these basic motifs for their binding to PI(4,5)P$_2$-containing membranes, we expressed wild-type and mutant GST fusion proteins of Tal-H and analyzed their binding to reconstituted liposomes mimicking the cytosolic leaflet of the plasma membrane by surface plasmon resonance (SPR; Zimmermann et al., 2002; Mortier et al., 2005). Liposomes were composed of 10% PI(4,5)P$_2$, 30% phosphatidylcholine (PC), 40% phosphatidylethanolamine (PE), and 20% phosphatidylserine (PS), and purified GST–Tal-H was perfused at 0.5 µM concentration. In this assay, Tal-H bound to PI(4,5)P$_2$, although to a lesser extent than the pleckstrin homology domain of PLC-δ, which was used as a positive control (Fig. S4 B). In addition, point mutations of the basic patch in Tal-F2 (K272A/K274Q/R277E) or pair-wise mutations of the Lys residues of the basic finger in Tal-F3 (K320A/K322A; K322A/K324A) reduced Tal-H association with the PI(4,5)P$_2$-containing lipid surface up to sixfold, as measured by the response units at equilibrium (Fig. 3 D). This identified a PI(4,5)P$_2$-binding ridge on the surface of Tal-H spanning across the F2 and F3 domains. However in FL-Tal, this basic ridge was partially shielded by the intramolecular interaction between Tal-F3 and
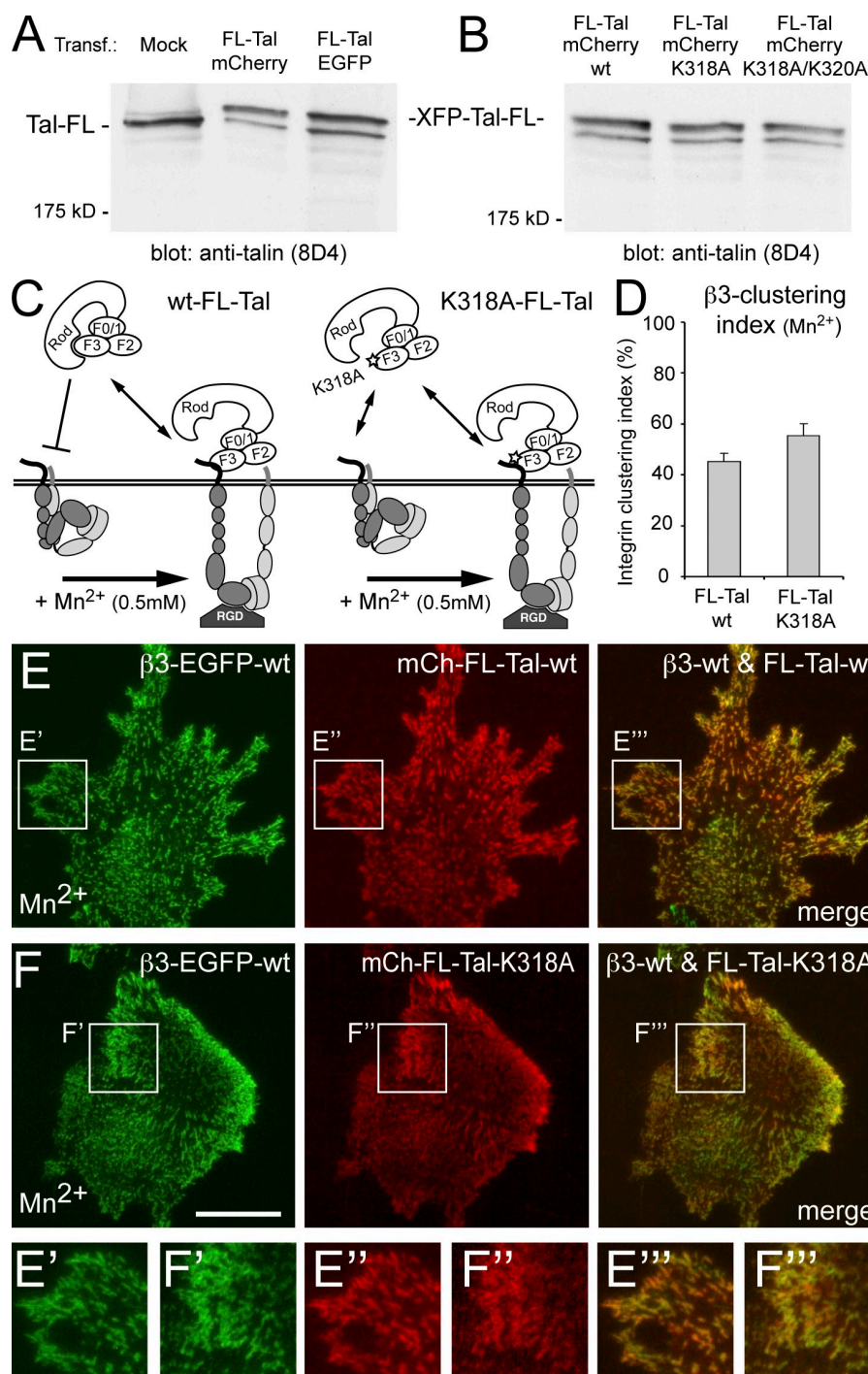
Figure 2. **The K318A mutation in FL-Tal increases β3-integrin clustering.** (A and B) Western blots of equivalent amounts of cell lysates probed with an anti-Tal mAb from wild-type (wt) or mutant mCherry– or EGFP–FL-Tal–transfected B16F1 cells. (C) Schematic view of $Mn^{2+}$-induced integrin activation and association with wild-type or K318A FL-Tal. (D) Integrin clustering index (percentage of pixels with >200 gray levels) of wild-type and K318A FL-Tal–transfected cells ($n = 4$; SEM). (E and F) Representative TIRF images of $Mn^{2+}$-stimulated B16F1 cells grown on serum-coated coverslips and double transfected with β3-EGFP-integrin (E and F) and wild-type (E) or K318A mCherry (mCh)–FL-Tal (F). Magnified views of the boxed areas are shown in E′–E‴ and F′–F‴. Bar, 20 µm.

Tal-R, proposing a PI(4,5)P$_2$-dependent regulation of Tal activation at the level of Tal-F3.

### Integrin clustering requires K$^{324}$ in Tal-F3 and the PI(4,5)P$_2$-binding sites in Tal-F2

To test the role of these PI(4,5)P$_2$-binding sites in Tal-H for integrin clustering, we expressed β3-EGFP-integrin with wild-type or mutant forms of ECFP–Tal-H (Fig. S4 C) in B16F1 cells and induced integrin clustering by $Mn^{2+}$ addition. The basic patch mutation in Tal-F2 (K272A/K274Q/R277E) blocked the capacity of Tal-H to increase $Mn^{2+}$-induced integrin clustering above control levels (Fig. 4, C and E). Similarly, the K322A/K324A mutant of Tal-H failed to increase integrin clustering (Fig. 4, B and E). In contrast, the PI(4,5)P$_2$ binding–deficient K320A/K322A mutant of Tal-H induced integrin clustering comparable with wild-type Tal-H (Fig. 4, A and E). Similarly, the double mutant K318A/K320A at the putative Tal-R–binding site did not block integrin clustering. Surprisingly, the R358A mutation, which abrogates integrin activation and binding of GST–Tal-H to the W$^{739}$/NPLY$^{747}$ motif (García-Alvarez et al., 2003), induced efficient integrin clustering (Fig. 4, D and E).
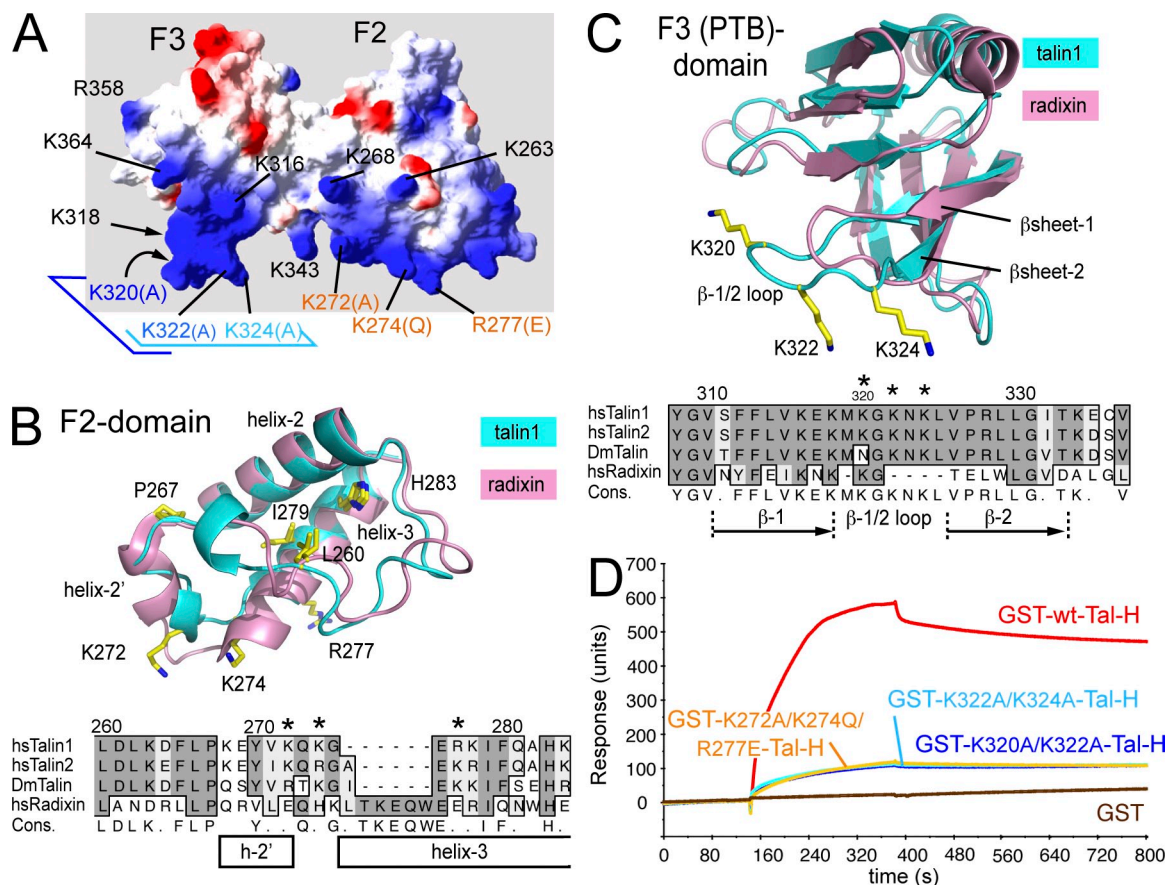
Figure 3. **The F2 and F3 domains of Tal-H contain PI(4,5)P$_2$-binding sites.** (A) Electrostatic surface map of the Tal-F2/3 structure (García-Alvarez et al., 2003) showing basic (blue) and acidic (red) amino acids. Mutations of basic amino acids are indicated in brackets. (B and C) Structure and sequence comparison of the F2 (B) and F3 (phosphotyrosine binding [PTB]) domain (C) of Tal1 (cyan) and radixin (pink). Basic motifs are indicated by asterisks, and conserved residues are shown in the structure. Note the basic patch in Tal-F2, replacing a turn of helix 3 of radixin (B) and the extended loop between β-sheets 1 and 2 in Tal-F3 (C). In the sequence alignments, identical and similar amino acids are indicated by dark and light gray shading, respectively. (D) SPR analysis of 0.5 µM GST–Tal-H binding to reconstituted liposomes composed of 10% PI(4,5)P$_2$, 30% PC, 40% PE, and 20% PS. Note that mutations of the basic residues in Tal-F2 and/or Tal-F3 reduce PI(4,5)P$_2$ binding.

These results demonstrate overlapping roles for PI(4,5)P$_2$ binding and integrin clustering for $K^{324}$ in Tal-F3 and the basic patch in Tal-F2. However, residues $K^{320}$ and $K^{322}$ in Tal-F3 were primarily involved in PI(4,5)P$_2$ binding, potentially regulating Tal-R association together with $K^{318}$ (Fig. 4, F and G). Therefore, the PI(4,5)P$_2$-binding ridge in Tal-H serves three functions: (1) regulating autoinhibitory binding to Tal-R, (2) inducing PI(4,5)P$_2$-containing membrane association, and (3) supporting integrin clustering.

## MP acidic residues (integrin E$^{726}$ and E$^{733}$) are involved in integrin activation

In contrast to Tal-F2, in which PI(4,5)P$_2$-binding activity correlates directly with integrin clustering, it appears that the basic loop ($K^{318}$–$K^{324}$) in Tal-F3 serves multiple functions. Besides PI(4,5)P$_2$ binding and autoinhibitory interaction with Tal-R (Goksoy et al., 2008; Goult et al., 2009), this loop has also been implicated in integrin activation (Wegener et al., 2007). To identify so far unrecognized cytoplasmic tail residues that are involved in binding to the basic loop of Tal-F3 (e.g., $K^{324}$), we screened MP domain mutants of β3-integrin for defects in Mn$^{2+}$-induced clustering.

First, the integrin activation capacity of these β3-EGFP-integrin mutants was determined by their ability to bind a snake venom–derived RGD-containing integrin ligand, SKI-7 (Ballestrem et al., 2001; Legler et al., 2001), by FACS. In comparison with wild type, the activating D723A mutation, which abrogates the inhibitory charge–charge interaction with $R^{995}$ of the integrin α subunit, increased binding to soluble integrin ligands by twofold. In contrast, mutations at the conserved NPLY (Y747A mutant) and MP aromatic motif (F730A) reduced binding of soluble integrin ligands. In addition to these established mutants, we identified two acidic residues, $E^{726}$ and $E^{733}$, which upon mutation (E726K and E733K), resulted in the perturbation of integrin ligand binding (Fig. 5, A and B).

To analyze the Tal-H–binding capacity of these newly identified acidic residues, we performed an integrin pull-down assay with a GST–Tal-H fusion protein. To assure that the proximity of the clasped α-integrin tail would not interfere with GST–Tal-H binding at the MP acidic residues, we combined the acidic mutants with the D723A mutation. When compared with wild-type β3-EGFP-integrin, both mutations at the conserved W/NPLY as well as the MP
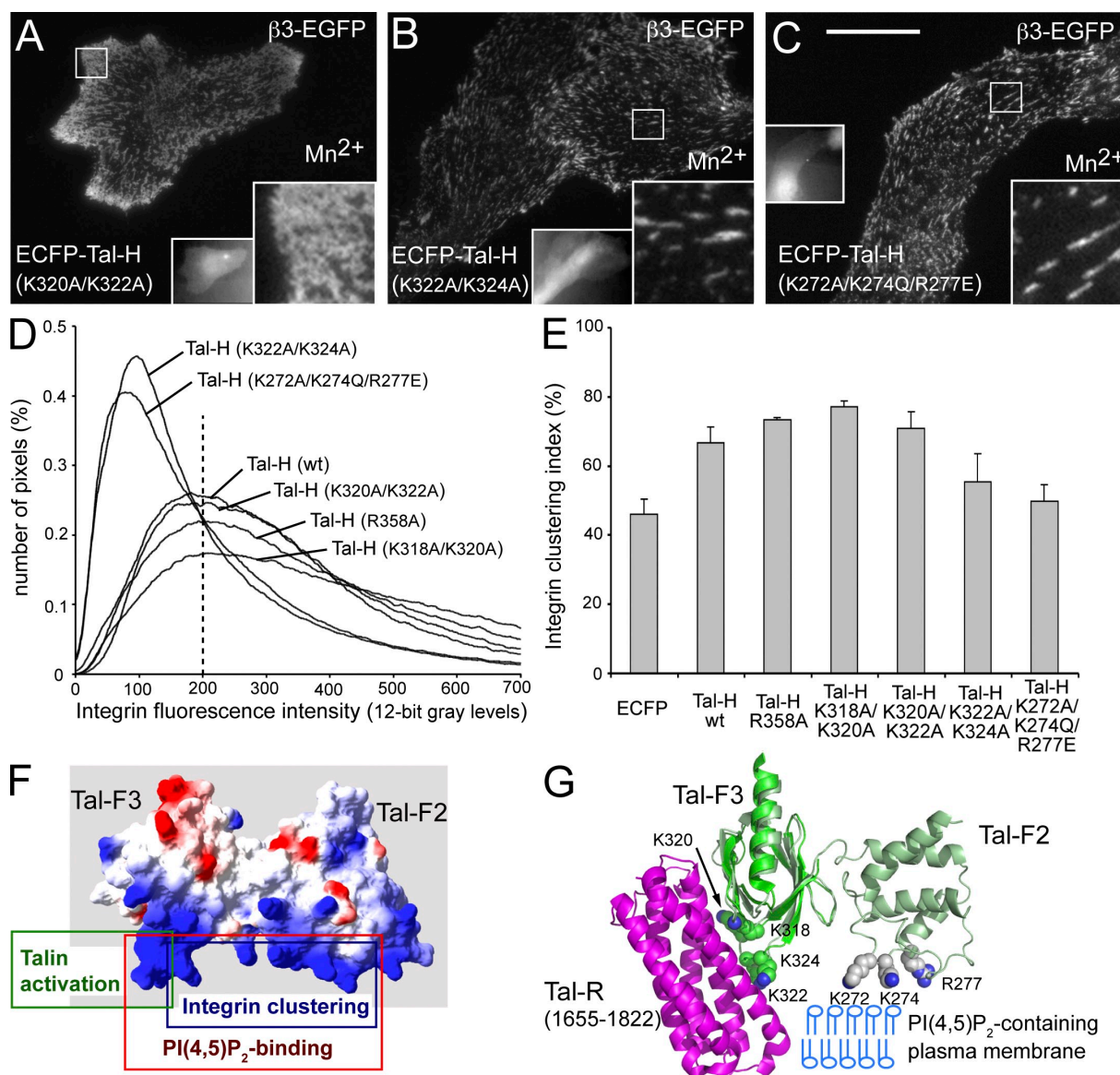
Figure 4. **Mutations in the PI(4,5)P₂-binding sites of Tal-H affect integrin clustering.** (A–C) Representative TIRF images (EGFP channel) of Mn²⁺-stimulated B16F1 cells grown on serum-coated coverslips and double transfected with β3-EGFP-integrin and ECFP–Tal-H carrying PI(4,5)P₂-binding mutations K320A/K322A (A), K322A/K324A (B), and K272A/K274Q/R277E (C). Magnified views of the boxed areas and ECFP–Tal-H expression are shown in the insets. (D and E) Averaged (n > 25) intensity histograms (D) and mean clustering index (n > 3; SEM; E) of β3-EGFP-integrin fluorescence as a function of Tal-H expression. The vertical dashed line in D represents the fluorescence intensity threshold (>200 12-bit gray levels) that was used to calculate the integrin clustering index. (F) Scheme of basic regions involved in Tal-R interaction, PI(4,5)P₂ binding, and integrin clustering. (G) Overlay of the proposed structure of the Tal-R–Tal-F3 complex (PDB ID 2KGX; Goult et al., 2009) with the Tal-F2/3 structure (PDB ID 1MK7; García-Alvarez et al., 2003), indicating PI(4,5)P₂ (K²⁷², K²⁷⁴, R²⁷⁷, K³²², and K³²⁴) as well as Tal-R–binding residues (K³¹⁸, K³²⁰ [hidden], K³²² [hidden], and K³²⁴; Goult et al., 2009). wt, wild type. Bar, 20 μm.

acidic motif prevented the biochemical interaction with GST–Tal-H (Fig. 5 B).

**Tal-H–induced clustering requires integrin tail residues E⁷²⁶ and E⁷³³ but not Y⁷⁴⁷ or F⁷³⁰**

To test whether a defect in integrin activation was functionally coupled to a defect in integrin clustering, we analyzed the aforementioned integrin activation mutants for defects in Tal-H–induced integrin clustering. When compared with the maximal clustering response of wild-type integrin, the activation mutants Y747A and F730A as well as the W739A/Y747A mutant (not depicted) kept the full capacity to form Tal-H–

dependent integrin clusters in the presence of Mn²⁺ (Fig. 5, D–F). Although surprising, this result was consistent with the unperturbed clustering activity of R358A mutant Tal-H. In contrast, both the E726K and E733K integrin mutations alone as well as the double mutant E726K/E733K or E726A/E726A (not depicted) failed to increase their clustering index when coexpressed with wild-type Tal-H (Fig. 5, G–I). This divided the integrin activation mutants in two classes: (1) one subset that clustered with Tal-H once integrin activation was induced by Mn²⁺ treatment (integrin Y747A and F730A) and (2) mutants that failed to cluster with Tal-H irrespective of integrin activation (integrin E726K and E733K).
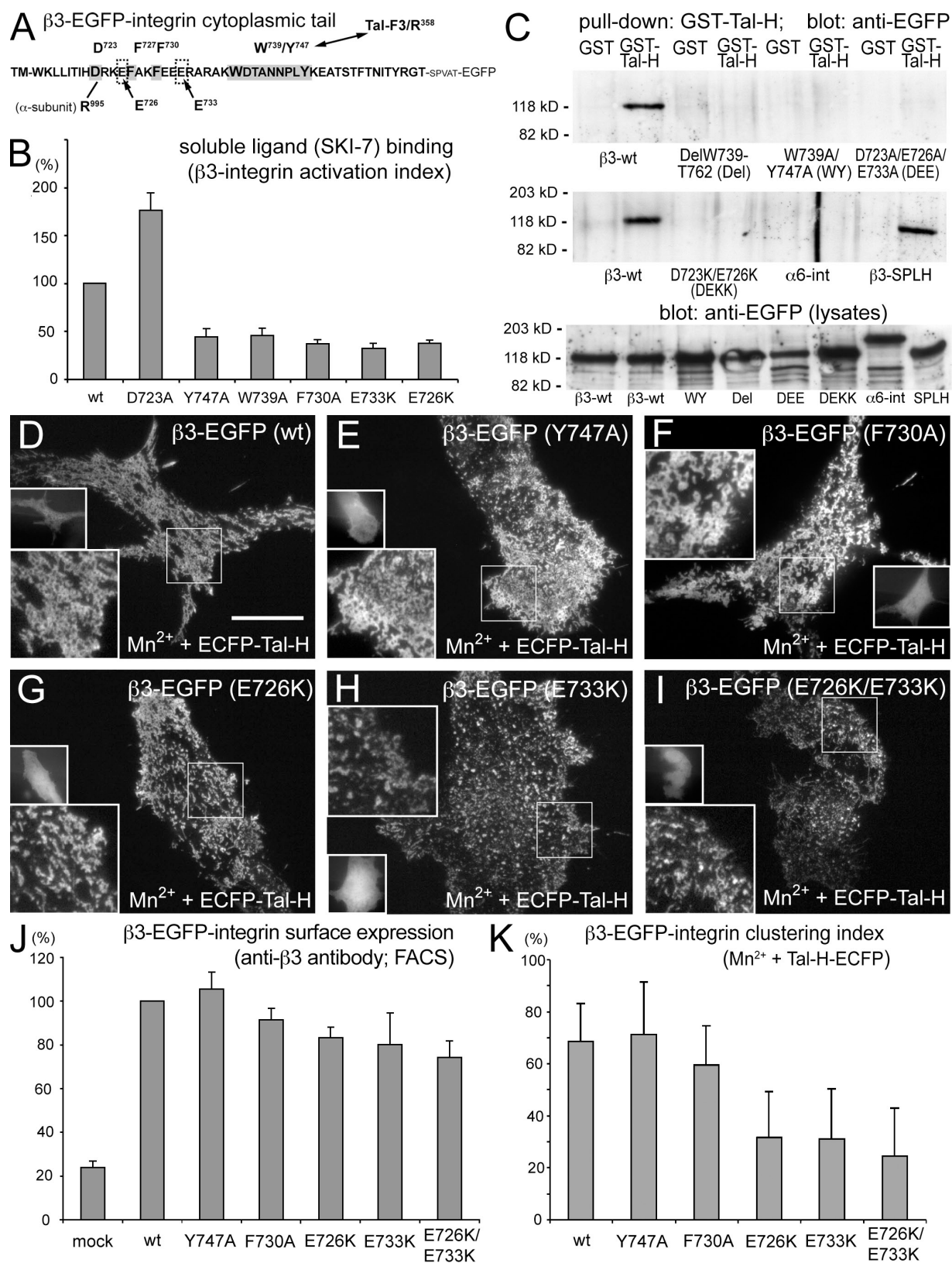
Figure 5. **Mutations of E[726] and E[733] affect integrin activation, Tal-H binding, and Tal-H–dependent integrin clustering.** (A) β3-EGFP-integrin cytoplasmic tail sequence with critical amino acids involved in integrin activation. (B) Soluble integrin ligand binding capacity (integrin activation index; $n > 3$; SEM) of different integrin mutants. (C) GST–Tal-H pull-down of wild-type (wt) and mutant β3-EGFP-integrins from lysates of transiently transfected COS-7 cells, involving DelW739-T762, W739A/Y747A, D723A/E726A/E733A, and D723K/E726K and as controls, α6-EGFP-integrin and the high-affinity NPLY integrin mutation (SPLH) according to Wegener et al. (2007). (D–I) Representative TIRF images (EGFP channel) of Mn^{2+}-stimulated B16F1 cells cotransfected with wild-type ECFP–Tal-H (insets) and wild-type (D) or mutant β3-EGFP-integrin Y747A (E), F730A (F), E726K (G), E733K (H), or E726K/E733K (I) and cultured on serum-coated coverslips. (J) Mean cell surface reactivity with anti–β3-integrin mAb ($n > 3$; SEM), as measured by FACS. Note that endogenous
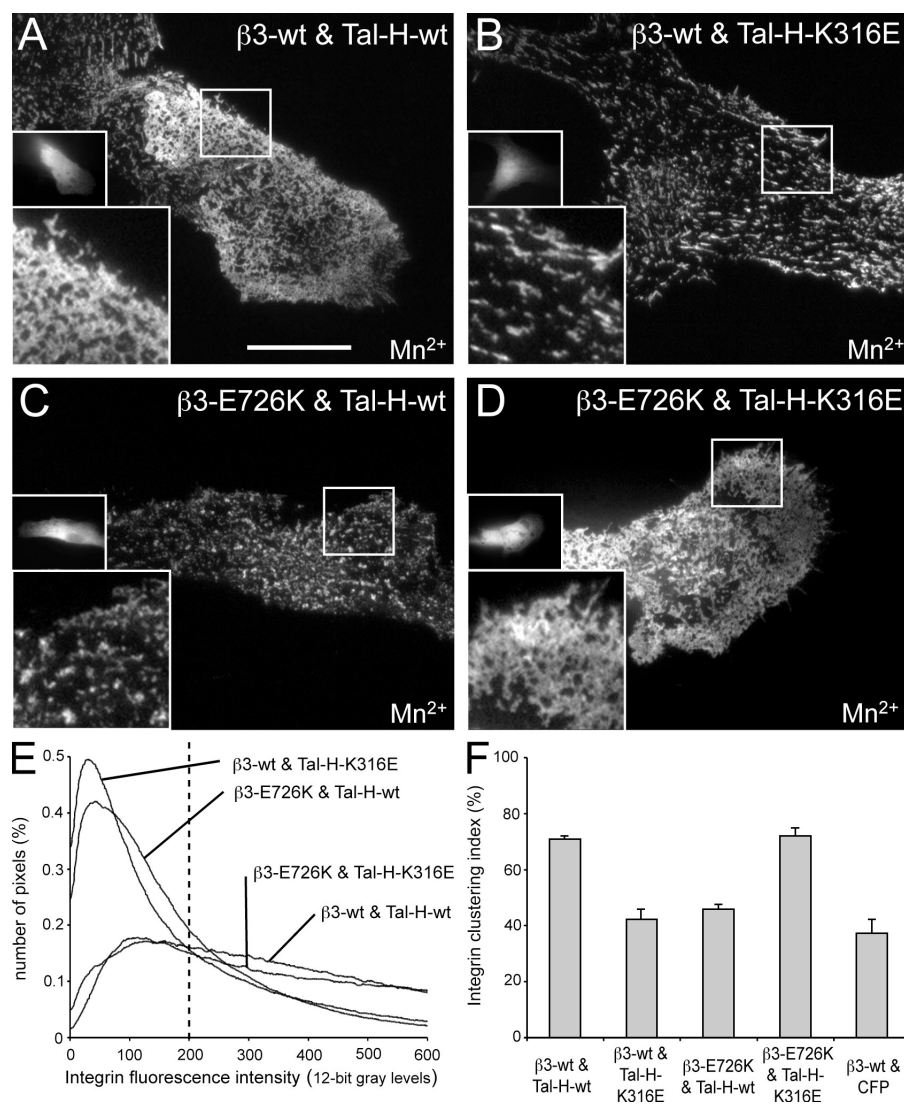
Figure 6. **Complementation of integrin clustering by charge-inversion mutants.** (A–D) Representative TIRF images (EGFP channel) of $Mn^{2+}$-stimulated B16F1 cells cultured on serum-coated coverslips and coexpressing wild-type (wt; A and B) or E726K mutant (C and D) β3-EGFP-integrin together with wild-type (A and C) or K316E mutant (B and D) ECFP–Tal-H. Magnified views of the boxed areas and ECFP–Tal-H expression by epifluorescence are shown in the insets. Note the extensive integrin clustering in the wild-type/wild-type (A) and E726K/K316E condition (D). (E) Averaged ($n > 25$) histograms of cells as shown in A–D. The dashed vertical line indicates the threshold used to calculate the integrin clustering index. (F) Mean integrin clustering index ($n > 3$; SEM) of conditions as in A–D. Bar, 20 µm.

## Direct Tal-H (K$^{316}$) and integrin (E$^{726}$) interactions in Mn$^{2+}$-induced integrin clusters

Considering the crucial role of the NPLY$^{747}$ motif in biochemical Tal-H binding assays, the formation of Mn$^{2+}$-induced, Tal-H–dependent clusters of the Y747A mutant was unexpected. One critical difference between the two assays is the presence of the plasma membrane, which could provide a scaffold for presently unknown integrin- or Tal-binding adapter proteins. Alternatively, PI(4,5)P$_2$ binding could orient Tal-H at the membrane to select for certain integrin interaction motifs (MP acidic residues) while reducing affinity to others that are prevalent for binding in solution (NPLY$^{747}$; F$^{730}$).

To distinguish between an indirect, but Tal-H dependent, from a direct interaction between Tal-H and integrins, we analyzed whether the acidic residues E$^{726}$ and E$^{733}$ could interact with complementary basic residues in Tal-H. Therefore,

charge inversion mutants E726K and E733K were tested for complementation with different Tal-H mutants carrying K to E mutations. Among the tested Tal-H mutants (e.g., K364E), none demonstrated complementation with the E733K β3-integrin mutant. However, the K316E mutation, although showing by itself a clustering defect and located at the proximal portion of the basic loop in Tal-F3, complemented the defect of the E726K mutation (Fig. 6). Coexpression of individual mutants with their respective wild-type counterpart failed to increase Mn$^{2+}$-induced integrin clustering (Fig. 6, B, C, and F). However, coexpression of both mutants (E726K and K316E) resulted in the formation of integrin clusters comparable with wild type (Fig. 6, A, D, and F). This demonstrates that Tal-H–integrin binding is direct, involving a charge–charge interaction between residues E$^{726}$ (integrin) and K$^{316}$ (Tal), identifying a new binding interface which is critical for Tal-dependent β3-integrin clustering.

---

β3-integrin levels correspond to 22% of wild-type β3-EGFP-integrin–transfected cells. (K) Mean clustering index ($n > 25$ cells; SD) taken from one representative out of three similar experiments. Bar, 20 µm.

Figure 7. **Complementation of focal adhesion formation by E726K β3-integrin and K316E FL-Tal.** (A–L) Representative TIRF images of transiently transfected B16F1 cells cultured on serum-coated coverslips in the absence of $Mn^{2+}$. Wild-type (wt; A and D) and E726K mutant (G and J) β3-EGFP-integrin were co-expressed with either wild-type (B and H) or K316E mutant (E and K) mCherry (mCh)–FL-Tal. The merged images demonstrate perfect colocalization in large focal adhesions in the wild-type/wild-type (C) and E726K/K316E (L) conditions. (E) In contrast, K316E FL-Tal was inefficiently recruited to focal adhesions in the presence of wild-type integrins. (G–I) Similarly, the E726K β3-integrin perturbed efficient cell spreading, causing irregular cell shapes and recruitment only to small focal adhesions. (M) Per cell quantification of the ratio of integrin to Tal fluorescence within focal adhesions. Each point corresponds to the mean of 5–15 contacts per cell. The horizontal bar represents the mean and SD of $n > 20$ cells. (N) Mean β3-EGFP-integrin fluorescence in focal adhesions, which is reduced for the E726K mutant integrin ($n > 20$ cells; mean and SD of 300–400 contacts per condition). Bar, 20 µm.
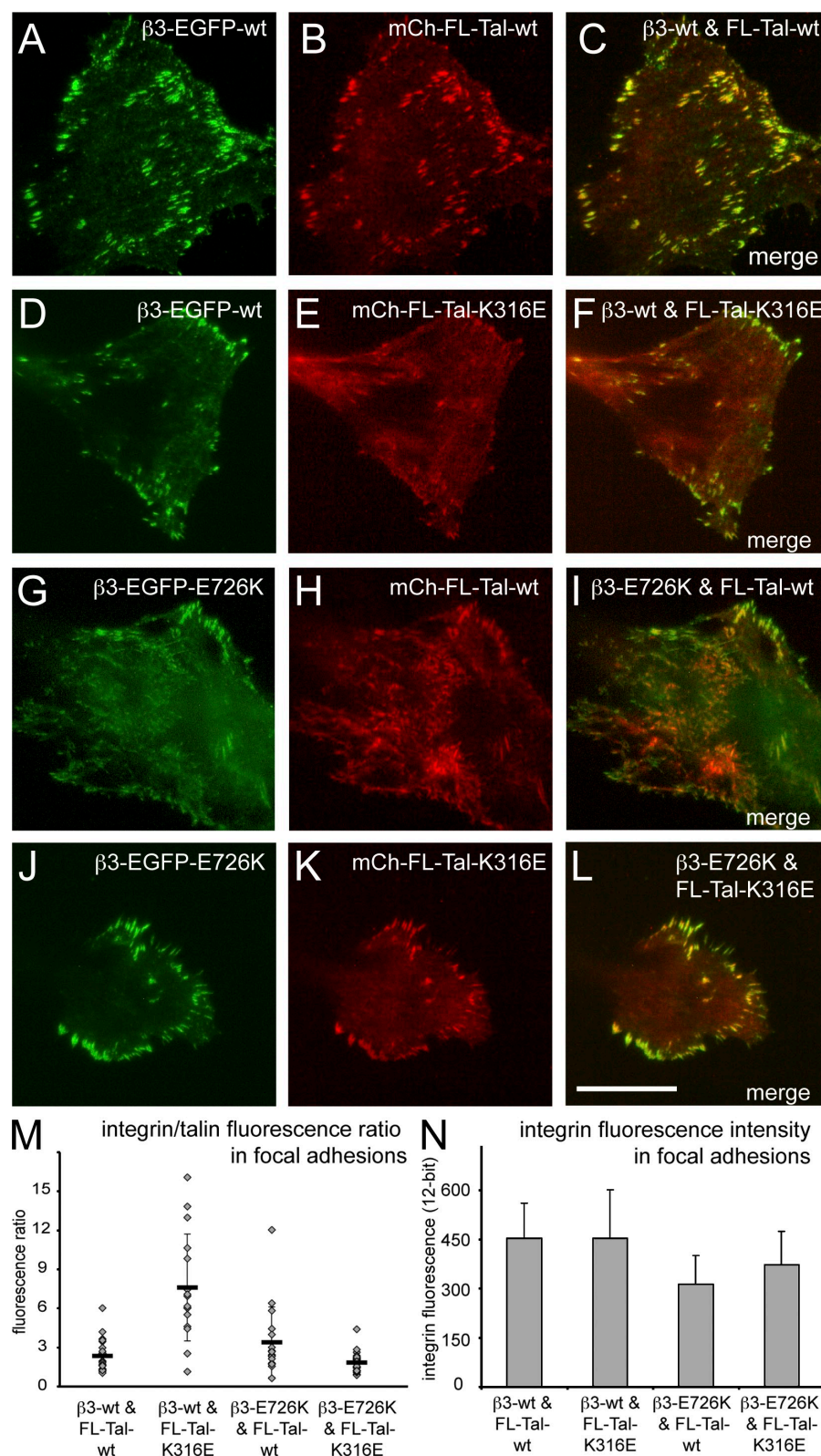
To demonstrate that this $E^{726}$–$K^{316}$ integrin–Tal interaction is also relevant for focal adhesion formation in the absence of $Mn^{2+}$, we examined complementation between the E726K integrin and the K316E mutant of FL-Tal. Coexpressing both mutants resulted in their perfect colocalization in large peripheral focal adhesions comparable with cells transfected with wild-type constructs (Fig. 7). In contrast, the expression of the E726K mutant integrin together with wild-type Tal reduced the recruitment of this integrin to focal adhesions. Similarly, K316E FL-Tal was not efficiently recruited into focal adhesions
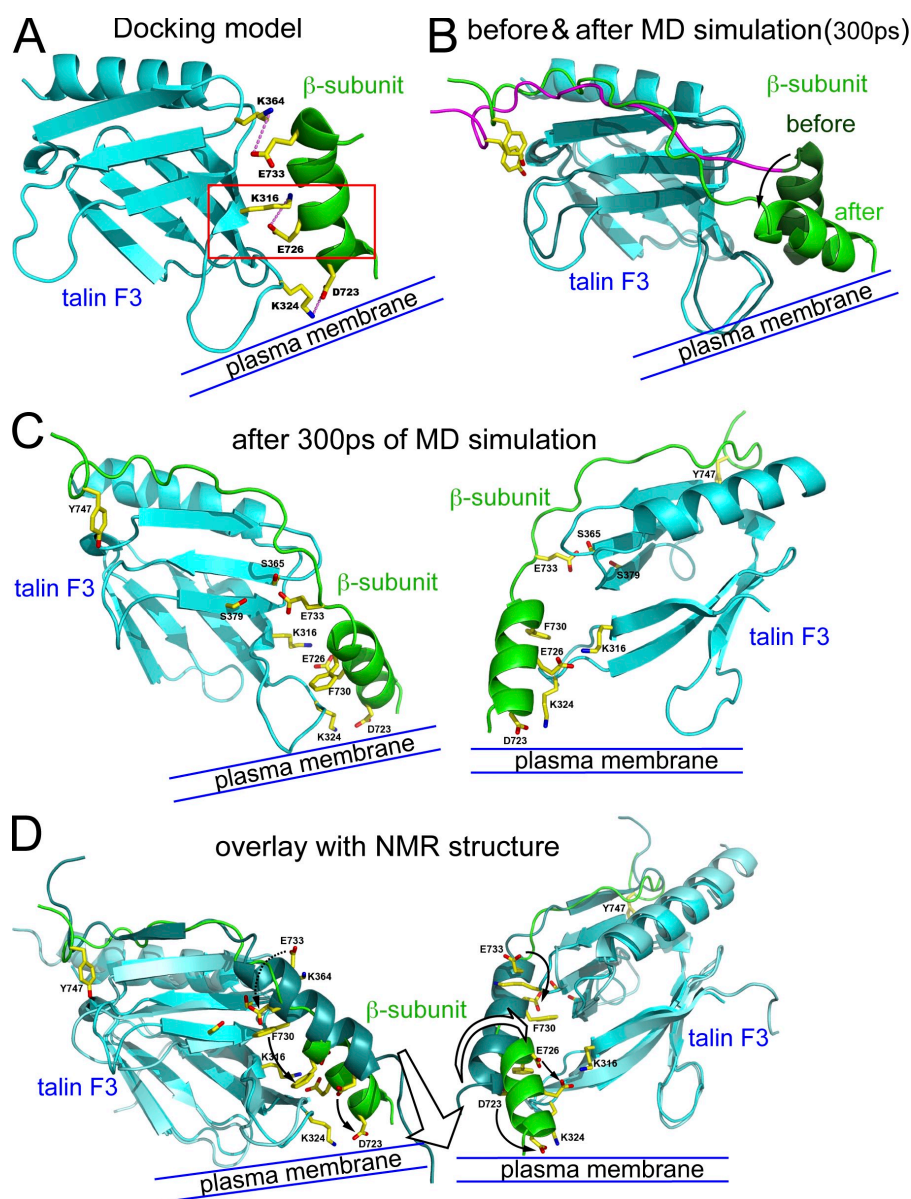
Figure 8. **Docking and MD analysis of the integrin–Tal interface.** (A) Side view of the MP helix of β3-integrin docked to Tal-F3, revealing putative charge–charge interactions (dotted lines) of residues required for Tal-dependent integrin clustering ($D^{723}$–$K^{324}$; $E^{726}$–$K^{316}$; $E^{733}$–$K^{364}$). (B) MD analysis starting from the model in A, after manual connection (magenta) to the Tal-F3–bound $W^{739}$/$NPLY^{747}$ motif. Snapshot after 300 ps of MD analysis, showing the position maintained for another 1500 ps. (C) Details of peptide position at 300 ps, indicating amino acids involved in interactions between $D^{723}$–$K^{324}$; $E^{726}$–$K^{316}$; $F^{730}$–$L^{325}$ ($L^{325}$ not depicted) and $E^{733}$ with $S^{365}$, $S^{379}$, and $Q^{381}$. A PDB file of this model is available in the supplemental data. (D) Overlay and shifts in localization (arrows) of relevant amino acids between the NMR-derived model (dark green; Wegener et al., 2007) and the structure shown in C (light green).

expressing wild-type integrin, resulting in a strong reduction of the integrin to Tal ratio in focal adhesions (Fig. 7). This proposes a critical function for the $E^{726}$–$K^{316}$ integrin–Tal interaction for the stability and maintenance of focal adhesions.

## Computational analysis of the Tal-F3–integrin binding interfaces

Neither the published structures of Tal-F2/3 fused to a β3-integrin tail fragment (García-Alvarez et al., 2003) nor the nuclear magnetic resonance (NMR) structure of Tal-F3 associated to a chimeric peptide containing the MP β3-integrin tail (Wegener et al., 2007) revealed the existence of a salt bridge between $K^{316}$ and $E^{726}$. Therefore, we decided to further define the binding interface between Tal-H and the MP $E^{726}$/$E^{733}$ integrin motif with computational analysis. First, we applied a peptide-docking algorithm, using the Tal-F2/3 crystal structure as the fixed model combined with the NMR structure–derived MP α-helix of β3-integrin as the mobile molecule (Eisenstein et al., 1997;

García-Alvarez et al., 2003; Vinogradova et al., 2004). In the model with the highest score (Fig. 8 A), we obtained charge–charge interactions between the integrin residues $D^{723}$, $E^{726}$, and $E^{733}$ with the Tal residues $K^{324}$, $K^{316}$, and $K^{364}$, respectively, and hydrophobic contacts between $F^{730}$ and $L^{325}$ (not depicted). Because the mutation of $K^{324}$ (K324E or K322A/K324A) blocked Tal-H–induced clustering of the D723A or D723K mutation, we propose that in addition to $PI(4,5)P_2$ binding, $K^{324}$ interacts with $D^{723}$ to stabilize integrin clusters. In contrast, the K364E mutant in Tal-H did not correct the clustering defect of the E733K mutant, suggesting that the $K^{364}$–$E^{733}$ interaction is not involved in integrin clustering.

To further evaluate our docking model, molecular dynamics (MD) simulations were conducted. For this, the integrin sequence was manually modeled between the docked MP helical domain and the Tal-bound $W^{739}$/$NPLY^{747}$ motif obtained from the crystal structure of the Tal-F2/3–integrin tail chimera (Fig. 8 B, magenta; García-Alvarez et al., 2003). Within 200 ps

of MD analysis, the position of the MP helix shifted slightly to assume a stable position for ~1.5 ns before progressive dissociation (a snapshot of this position taken at 300 ps is shown in Fig. 8, B and C). Although tilted in respect to the initial docking model, interactions between $F^{730}$ and $L^{325}$, between $E^{726}$ and $K^{316}$, and between $D^{723}$ and $K^{324}$ were maintained (Fig. 8, B and C). In contrast, the side chain of $E^{733}$ shifted considerably to localize into a hydrophilic pocket formed by $S^{365}$, $S^{379}$, and $Q^{381}$, loosing contact with $K^{364}$ (Fig. 8 C). The critical role of $K^{324}$ in Tal-H to induce integrin clustering (Fig. 4) agreed well with the maintenance of the $K^{324}$–$D^{723}$ contact during our simulation.

The comparison of our Tal–integrin interaction model with the NMR-based model of the Tal–integrin complex in solution (Wegener et al., 2007) revealed a membrane-directed shift and clockwise rotation (~50°) of the MP integrin helix, burying residue $D^{723}$ within the integrin–Tal interface (Fig. 8 D). The shift and rotation of the MP helix was also illustrated by the movement of $F^{730}$ to take the place occupied by $F^{727}$ in the NMR model (Wegener et al., 2007). However, the side chain of $E^{733}$ rotated from a solvent-exposed position in the vicinity of $K^{364}$ into the hydrophilic pocket ($S^{365}$, $S^{379}$, and $Q^{381}$; Fig. 8 D). This latter interaction would correlate with the critical role in integrin activation of both residue $E^{733}$ and the hydrophilic pocket described by Wegener et al. (2007).

Because residue $E^{733}$ plays a critical role in integrin activation and clustering, we analyzed whether the proximity to residue $K^{364}$ was relevant to Tal-H–integrin interaction. To remove a potential steric hindrance and electrostatic interaction with residue $E^{733}$, the side chain of $K^{364}$ was truncated (K364A). Consistent with a facilitated inward movement of $E^{733}$, the K364A mutation increased Tal-H–induced integrin clustering in the absence of $Mn^{2+}$ from 27 to 53% (Fig. S5). This result proposes the existence of two functionally distinct Tal–integrin binding interfaces at the MP domain, which are used in respect to the activation state of Tal and integrins. It further proposes that residue $K^{364}$ creates an energy barrier for binding site switching, preventing premature access of Tal to the inhibitory salt bridge ($D^{723}$–$R^{995}$) under suboptimal conditions.

Furthermore, MD simulations of the K364A mutant, starting from our refined docking model (Fig. 8 C), revealed an upward shift of the MP helix eventually lodging in a binding state comparable with the NMR-derived binding model (Fig. 8 D and Fig. S5). Removing the large $K^{364}$ side chain appeared to facilitate the transition from the Tal-H–integrin interaction in solution (Wegener et al., 2007) to the state required for integrin clustering (Fig. 8 D), probably by reducing the energy barrier for switching the bulky aromatic side chains of $F^{730}$ between adjacent hydrophobic pockets. Therefore, we propose a switch from an $NPLY^{747}$-dependent mode of Tal–integrin interactions in solution required for initiation of integrin activation to an $E^{726}$/$E^{733}$-dependent interaction, which allows integrins to form clusters.

## Discussion

Cell migration and the adaptation to mechanical tension require the dynamic remodeling of integrin-dependent adhesion sites. Despite the physiological importance of this system, neither the biochemical nor physical mechanisms that control integrin clustering, which is an integral step in the maturation of adhesion sites, have been understood (Geiger and Bershadsky, 2001; Wehrle-Haller and Imhof, 2002; Zhang et al., 2008; Vogel and Sheetz, 2009). Based on our experiments, we propose a mechanism for Tal activation at the plasma membrane, subsequently promoting integrin unclasping and the formation of integrin clusters by interaction at an acidic MP binding motif.

### Binding to PI(4,5)P₂-containing membranes unlocks Tal's autoinhibition

$PI(4,5)P_2$-mediated Tal binding to membranes appears to be critical for Tal activation (Martel et al., 2001). Based on our findings and the recently proposed Tal-F3–Tal-R (1,655–1,822) complex (Goult et al., 2009), we propose that $PI(4,5)P_2$-containing membranes compete with Tal-R as a binding partner for residues $K^{318}$, $K^{320}$, and $K^{322}$ in the basic finger of Tal-F3, thereby abolishing the autoinhibition of Tal by releasing the intramolecular clamp between Tal-H and Tal-R. In turn, amino acids $K^{316}$ and $K^{324}$ that bind the MP acidic motif in integrins get exposed. However, the $NPLY^{747}$-binding pocket in Tal-F3 appears not to be hidden by Tal-R binding (Goksoy et al., 2008; Goult et al., 2009), opening the interesting perspective that MP β-integrin residues (e.g., $E^{733}$) contribute to Tal unclasping by competing with acidic residues from Tal-R for binding to Tal-F3. The observed Tal-H binding to $PI(4,5)P_2$-containing membranes (Fig. 3) confirms SPR results obtained with pure $PI(4,5)P_2$-coated surfaces (Goksoy et al., 2008). Consistent with a competition between $PI(4,5)P_2$ and Tal-R binding at the basic loop in Tal-F3, these authors demonstrated a direct interference of $C_8$-$PI(4,5)P_2$ micelles with the Tal-F3–Tal-R (1,654–2,344) interaction. However, only small chemical shift perturbations were detected between $C_4$-$PI(4,5)P_2$ micelles and Tal-F3 in solution, making it difficult to map the $PI(4,5)P_2$ binding interface on Tal-F3 (Goksoy et al., 2008). Both small spherical $C_4$-$PI(4,5)P_2$ micelles in contrast to flat $PI(4,5)P_2$-containing membranes as well as the use of only Tal-F3 and not Tal-F2/3 could have been responsible for detecting residue $Q^{374}$ (Goksoy et al., 2008) instead of the basic loop in Tal-F3 and basic pocket in Tal-F2 as the major $PI(4,5)P_2$ binding interfaces. In contrast, our data indicate that the entire $PI(4,5)P_2$-binding ridge spanning Tal-F2 and Tal-F3 would participate to dislodge Tal-R from the basic loop in Tal-F3, ultimately leading to the exposure of the MP integrin–binding site. In turn, removal or hydrolysis of $PI(4,5)P_2$ would result in Tal-H detachment from membranes, which would expect to return Tal to the autoinhibited state (Fig. 9).

### F2-mediated membrane interaction is required for integrin clustering

Using biochemical assays, it has been demonstrated that Tal-F3 binds to the $NPLY^{747}$ motif of integrins and that Tal-R contains a binding site for the MP region of integrins (García-Alvarez et al., 2003; Rodius et al., 2008; Gingras et al., 2009), proposing that the integrin–Tal interaction in living cells is mediated by these interfaces. However, when performed in a physiological membrane environment, neither the $NPLY^{747}$ nor the integrin-binding site in Tal-R was required for integrin clustering.

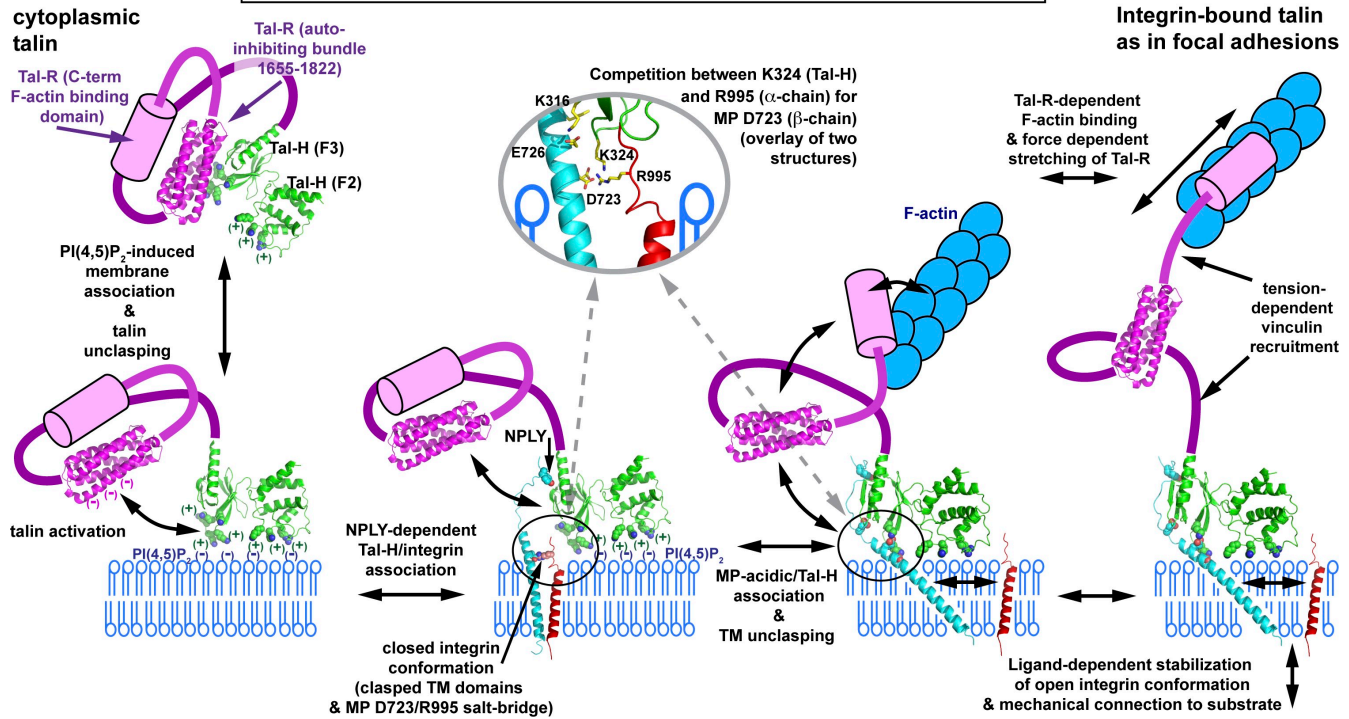**Biochemical and mechanical control of talin/integrin association**

Figure 9. **Mechanical and biochemical control of Tal–integrin association during focal adhesion formation.** Multiparametrical regulation of the integrin–Tal association. The autoinhibited form of Tal (top left) can interact with PI(4,5)P$_2$-enriched membranes, resulting in Tal-R dissociation from Tal-H (bottom left). In turn, PI(4,5)P$_2$-bound Tal-H associates with clasped integrin receptors via the NPLY motif of the cytoplasmic domain of β-integrins (middle left). Integrin transmembrane domain unclasping by the basic finger in Tal-F3 interacting with the MP acidic motif in the β-integrin tail, creating a competition between K$^{324}$ of Tal-H with R$^{995}$ of the α subunit for D$^{723}$ association. This competition is illustrated by the overlay of two exclusive structures (magnified inset; top middle). Stable Tal-H association with the MP acidic motif requires the open integrin conformation stabilized by integrin ligand occupancy (middle right). In the absence of F-actin, maintaining the Tal–integrin complex requires Mn$^{2+}$ or mutational activation of integrins (e.g., salt bridge mutation). In the presence of F-actin, the C terminus of Tal-R (pink tube) can be captured, potentially reducing the autoinhibitory interaction of Tal-R (1,655–1,822) with Tal-H (middle right). Force-dependent stretching of Tal-R creates new binding sites for vinculin, stabilizing the integrin–F-actin linkage, preventing Tal autoinhibition (right).

Instead, the PI(4,5)P$_2$-binding site in Tal-F2 was critical to maintain integrin clustering. Accordingly, short term extraction of PI(4,5)P$_2$ lipids with neomycin sulfate results in the dispersal of normal and Mn$^{2+}$-induced integrin clusters (Cluzel et al., 2005), indicating that the local composition and structure of the plasma membranes plays an important role in maintaining integrin clustering (Gaus et al., 2006). We propose that Tal-H binding to PI(4,5)P$_2$-containing membranes restricts rotational movement, favoring a Tal-H orientation, which optimizes interaction with the MP proximal acidic motif (D$^{723}$/E$^{726}$/E$^{733}$). Our data demonstrate that plasma membrane interactions determine hierarchies and binding strength of integrin adapters, which in turn stabilize the high-affinity conformation, favoring the formation of integrin clusters.

### Tal-H interaction with a new MP integrin motif, E$^{726}$ and E$^{733}$, promotes clustering independent of the NPLY motif

One critical step in integrin activation is the release of the intermolecular salt bridge between the β and α cytoplasmic tail residues D$^{723}$ and R$^{995}$ (in αIIbβ3), respectively (Hughes et al., 1996; Kim et al., 2009; Lau et al., 2009). Likewise, dominant integrin clustering is induced when this salt bridge is mutated (D723A; Ballestrem et al., 2001; Cluzel et al., 2005). Therefore,

it has been proposed that Tal-H interferes with this salt bridge during integrin activation (Wegener et al., 2007; Anthis et al., 2009). In accordance with these studies, our data provide evidence for a direct interaction between K$^{324}$ of the basic finger in Tal-F3 with D$^{723}$, maintaining a competitive interaction that efficiently shields the β cytoplasmic tail from reassociation with its α subunit (Fig. 9). Competition at D$^{723}$ also explains the crucial role of integrin occupancy for Tal recruitment (Miyamoto et al., 1995). Because ligand binding perturbs the inhibitory salt bridge (D$^{723}$–R$^{995}$) by outside-in regulation, it exposes residues D$^{723}$ and E$^{726}$ to stabilize Tal-H binding at the MP acidic motif. Furthermore, integrin clustering induced by the D723A mutation occurs even in the presence of the Y747A mutant but is blocked by mutations at either E$^{726}$ or E$^{733}$, phenocopying the clustering results obtained with Mn$^{2+}$ treatment (unpublished data).

Importantly, this further defines the differential functions of the NPLY$^{747}$ and the MP E$^{726}$/E$^{733}$ Tal-binding sites within integrin tails. The differential use of these motifs for integrin activation and subsequent clustering agrees with the mild muscle attachment defect observed in *Drosophila* embryos, in which only the former function is lost (Tanentzapf and Brown, 2006). Furthermore, in biological systems in which rapid integrin activation is crucial such as platelet activation, Tal-dependent inside-out activation of integrins requires the conserved NPLY

and MP aromatic motif (García-Alvarez et al., 2003; Tadokoro et al., 2003; Wegener et al., 2007). In contrast, in cells using force-dependent regulation of integrin-dependent anchorage, mutations affecting the inhibitory salt bridge, as for example in β1-integrins, are without consequence for the proper functioning of the organism (Czuchra et al., 2006). In addition, because Tal-induced clustering of NPLY mutant integrin can occur upon $Mn^{2+}$-stimulated outside-in activation, it is possible that this Tyr motif plays Tal-dependent as well as Tal-independent roles in the integrin-controlled cellular physiology (Czuchra et al., 2006). For example, both the Y747A and L746A β3-integrin mutants perturb Tal binding in vitro, affecting integrin activation, whereas only the former mutant exhibits a severe platelet aggregation phenotype (Petrich et al., 2007a).

### The Tal-H to Tal-R linkage provides mechanical control over the integrin–Tal complex

One of the consequences of Tal-H–dependent integrin clustering is the absence of vinculin recruitment and uncoupling from the F-actin network. However, Tal-R fragments interact with focal adhesions, using the C-terminal F-actin–binding motif (Franco et al., 2006; Gingras et al., 2008; Zhang et al., 2008). Accordingly, Tal-H is sufficient to maintain integrin-dependent anchorage of the spreading lamella in Tal-depleted cells, whereas FL-Tal (probably via Tal-R–dependent F-actin–vinculin association) forms the link to the actin cytoskeleton, allowing mechanosensing (Fig. 9; Franco et al., 2006; Zhang et al., 2008). Our results now provide the mechanism for this observation, involving $PI(4,5)P_2$-dependent dissociation of Tal-H from Tal-R allowing simultaneous binding of Tal-H to integrins/$PI(4,5)P_2$ and Tal-R to F-actin. The dual connected Tal (F-actin and integrin) can now respond to mechanical tension between immobilized integrin ligands and the actin cytoskeleton by recruiting vinculin to Tal-R, thereby increasing the stability of the integrin–Tal–F-actin linkage (Fig. 9; Hytönen and Vogel, 2008; del Rio et al., 2009).

To conclude, we present new protein–protein and protein–lipid interactions that provide a mechanism of FL-Tal–induced integrin clustering and F-actin connection. It is central that Tal-H can interact with $PI(4,5)P_2$-containing membranes as well as with the MP acidic motif in ligand-bound integrins, which are processes both tightly controlled by Tal-R association. Integrin clustering induced by Tal-H requires integrin activation and Tal unclasping, which initially happens without a force-bearing linkage between integrins and the cytoskeleton. However, during force-dependent maturation of focal adhesions, the F-actin–vinculin–Tal-R association regulates Tal-H exposure, allowing $PI(4,5)P_2$ interaction and clustering of ligand-bound integrins, determining mechanosensing and adhesion signaling.

## Materials and methods

### cDNAs and site-directed mutagenesis
The constructs encoding FL mouse β3-EGFP-integrin in pcDNA3 have been described previously (Ballestrem et al., 2001; Cluzel et al., 2005). Integrin point mutations were introduced by primer overlap extension and subsequently verified by automated sequencing. An integrin mutant with a high-affinity NPLY motif (SPLH) was constructed according to Wegener et al. (2007), in which the NPLY motif ($K^{738}$WDTANNPLY$^{747}$KEAT) was replaced by residues from the C terminus of PIPKI-γ ($K^{738}$WVYSPLHYSAT; modified residues underlined; de Pereda et al., 2005).

The head domain of human Tal1 (residues 1–435) was amplified with *PfuTurbo* DNA polymerase (Promega) from IMAGE clone 4615125 (obtained from GenBank/EMBL/DDBJ under accession no. BG428074), cloned into the XhoI and EcoRI sites of pECFP-C1 (Takara Bio Inc.), and swapped into pcDNA3 (ECFP–Tal-H) using the primers 5′-GATCTCGAGC-CATGGTTGCACTTTCACTG-3′ and 5′-TATGAATTCTATTGCTGCTGCAG-GACTG-3′. The same reverse primer and the XhoI-containing forward primer (5′-GATCTCGAGAGGGAGCACGAGACGCTG-3′) were used to amplify and to clone Tal-F2/3 (residues186–435) of human Tal1. Similarly, the respective forward (5′-AGACTCGAGCTTACGGTGTCTCCTTCTTC-3′) and reverse (5′-CATGAATTCTACAGCCCAAAGTGATCCTTG-3′) primers were used to clone Tal-F3 (residues 308–411). Mouse EGFP-tagged FL-Tal1 was obtained from A. Huttenlocher (University of Wisconsin School of Medicine, Madison, WI) and used to create a FL human/mouse Tal1 chimera at a conserved EcoRV site located at $I^{398}$ of human and mouse Tal1. ECFP–Tal-R in pcDNA3 (residues 1,073–2,541) was created by cloning the C-terminal rod fragment of mouse Tal1 at a unique XhoI site ($D^{1073}$) at the place of Tal-H. Tal-H and β3-EGFP-integrin mutations were introduced by primer overlap extension using *PfuTurbo* DNA polymerase. DNA sequence analysis was performed for all constructs to ensure error-free amplification and correct base replacement. Various EGFP- or mCherry-tagged variants of different Tal constructs were generated by exchanging fluorophores (Shaner et al., 2004), without detecting differences in integrin clustering performance. The GST–Tal-H fusion constructs used for the SPR and pull-down experiments were obtained by the insertion of PCR-amplified wild-type or mutated human Tal-H (1–435) into pGex-2T at the BamH1–EcoRI sites using the primers 5′-CCGAGATCTGCCATGGTTGCACTTT-CAC-3′ and 5′-TATGAATTCTATTGCTGCTGCAGGACTG-3′.

### Cell culture and transient transfections
Mouse B16F1 melanoma cells were grown in DME containing 10% FCS, Gln, and antibiotics, as previously described (Ballestrem et al., 2001). Transfections were performed with Jet Pei (Polyplus Transfection) according to the manufacturer's recommendation. After 6 h in Jet Pei–containing transfection solution, cells were detached and replated in plastic dishes or cultured on glass-bottom dishes in complete medium, providing serum-derived vitronectin as the αvβ3-integrin ligand. For spreading experiments on defined protein substrates, glass coverslips were coated for 1 h at room temperature with purified vitronectin, fibronectin, or laminin-1 diluted in PBS at the indicated concentrations, followed by washing and blocking of the coated surfaces with 1 mg/ml human serum albumin (Sigma-Aldrich). Integrin-expressing cells were detached with trypsin/EDTA, washed and blocked with trypsin inhbitor containing DME, and seeded in 1% human serum albumin containing DME.

### Measurement of integrin clustering and TIRF microscopy
48 h after transfection, activation with 0.5 mM $Mn^{2+}$ for 20 min in complete culture medium, followed by fixation for 10 min in 4% PFA/PBS and storage in PBS. TIRF microscopy was performed on a microscope (Axiovert 100M; Carl Zeiss, Inc.) equipped with a combined epifluorescence/TIRF adapter (TILL Photonics) and a 100× NA 1.45 objective (Carl Zeiss, Inc.). EGFP fusion proteins were excited with the 488-nm line of a 150-mW argon-ion laser (Reliant 150m; Laser Physics), and red dyes were excited with the 535-nm line of a 20-mW diode laser (Compass 215M-20; Coherent, Inc.). Openlab software (PerkinElmer) controlled image capture by a 12-bit charge-coupled device camera (Orca 9742-95; Hamamatsu Photonics) as well as the operation of the laser shutters and microscope. For publication, the background and contrast were adjusted using the "Level" command in Photoshop (Adobe).

Intensity histograms of cells were obtained from 12-bit images after background subtraction, and selection of the cell surface area was performed using MetaMorph software (MDS Analytical Technologies) and exported to Excel (Microsoft) for further analysis. Histograms were normalized in respect to the cell surface area and averaged ($n > 25$). The relative surface occupied by clustered integrins (expressed as a percentage) was obtained from intensity histograms by determining the sum of the pixels brighter than an arbitrary fluorescence intensity threshold of 200 (12 bit) gray levels, which was defined as the clustering index. The selection of the integrin clustering threshold at 200 gray levels, was based on the expression of clustering-deficient integrins such as the D119Y mutant (Cluzel

et al., 2005), which exhibit no fluorescent pixels above the threshold (clustering index of 0%).

To validate the integrin clustering analysis, we assured similar surface expression levels of the transfected wild-type and mutant EGFP-integrins by FACS (Fig. 5 J). Because of the characteristic shape of the fluorescence intensity histogram and the selection of the threshold value between the low- and high-intensity portion of the histogram, the measurement of the integrin clustering index was relatively insensitive to variations of cell surface integrin expression of certain integrin mutants. For each mutant and condition, experiments were repeated at least three times, and clustering was compared with internal standards obtained with wild-type constructs. Quantification was performed from triplicates (SEM) or from one representative experiment with SD of the clustering index of individual cells ($n > 25$).

Detection of F-actin and vinculin by TIRF microscopy was performed from 4% PFA/PBS–fixed and PBS-washed cells. After permeabilization and blocking in 0.1% Triton X-100 in 1% BSA/PBS, F-actin was detected with Texas red–phalloidin (Invitrogen), and vinculin was revealed by incubation with monoclonal antivinculin (clone VIN-11-5; Sigma-Aldrich) followed by Texas red–conjugated goat anti–mouse antibodies (Jackson Immuno-Research Laboratories, Inc.). Imaging was performed in PBS as indicated at the beginning of this section, and for publication, the contrast of images was adjusted using the "Level" command in Photoshop.

## Liposome preparation and SPR

Liposomes containing 10% $PI(4,5)P_2$ were produced and applied to the sensor chip as previously described (Zimmermann et al., 2002; Mortier et al., 2005). In brief, PC, PE, PS, and $PI(4,5)P_2$ or PI dissolved in chloroform at the appropriate concentrations (30:40:20:10) and dried under a stream of $N_2$. Liposomes were prepared by rehydration in 50 mM Hepes, pH 7.4, 450 mM NaCl, and 1 mM EDTA and repetitive freeze thawing and extrusion through two stacked 100-nm pore size polycarbonate filters. Liposomes were applied to a L1 lipophilic association chip on a Biacore 2000 (GE Healthcare) at 0.5 mM with a flow rate of 2 μl/min and washed with brief pulses of 10 mM NaOH. Purified GST–Tal-H fusion proteins at 0.5 μM in running buffer (20 mM Hepes, pH 7.4, and 150 mM NaCl) were perfused over liposomes containing 10% PI or $PI(4,5)P_2$ at a flow rate of 30 μl/min. After 4 min of association, the complex was allowed to dissociate. Sensograms were corrected for background association to 10% PI–containing vesicles.

## Flow cytometry and integrin activation analysis

B16F1 mouse melanoma cells were transiently transfected with β3-EGFP-integrin constructs. Transfected cells were analyzed for their expression of EGFP fluorescence and for cell surface–exposed or activated αvβ3-integrins using either a hamster anti–mouse β3-integrin mAb (BD) or the RGD-containing Kistrin-CD31 fusion protein (SKI-7) followed by a rat anti-CD31 mAb (GC51), respectively (Ballestrem et al., 2001; Legler et al., 2001). Primary or secondary antibodies were further detected with R-phycoerythrin–conjugated goat anti–mouse IgM + IgG + IgA or goat anti–rat IgG (SouthernBiotech). For each sample, $10^4$ events were acquired on a FACScan and analyzed by the CellQuest software (BD). The integrin activation index was determined from the SKI-7 to anti-β3 binding (geomean) ratio according to the following formula:

$$\text{Activation index} = \frac{\left(\text{SKI-7}\left(\text{EGFP}^+\right) - \text{SKI-7}\left(\text{EGFP}^-\right)\right)}{\left(\text{anti-β3}\left(\text{EGFP}^+\right) - \text{anti-β3}\left(\text{EGFP}^-\right)\right)},$$

where $\text{EGFP}^+$ indicates β3-EGFP-integrin–transfected cells and $\text{EGFP}^-$ indicates nontransfected control cells. The activation index (percentage) was normalized to wild-type β3-EGFP-integrin–transfected cells.

## Docking prediction

The docking prediction was performed using the protein–protein docking program *FTDOCK* (Eisenstein et al., 1997) on a dual-processor computer. The preliminary models were downloaded from the protein database and prepared for analysis. A monomeric Tal-F2/3 model was obtained from the PDB structure 1MK7 (García-Alvarez et al., 2003) by keeping only chain B. The MP helical domain of the integrin β3 cytoplasmic tail (residue 720–735) was prepared from the PDB structure 1S4X (Vinogradova et al., 2004). In docking calculations, global scan was performed using Tal as the static model and the helix of β3 cytoplasmic tail as the mobile molecule. The docking possibilities were ranked in terms of shape complementarity, electrostatics,

and empirical scores of residue level pair potentials. This result was subsequently filtered using knowledge acquired from mutational experiments, in this case, i.e., setting proximity constraints (4.5 Å) between $K^{316}$ (Tal) and $E^{726}$ (integrin). Three docking models satisfied the constraints, and the top one with the highest score was chosen as the final model (Fig. 8 A). Models were produced using PyMOL (DeLano Scientific).

## MD simulations

Initial protein coordinates for MD analysis were obtained by manually combining W/NPLY motif and MP helical domains using the program VMD (Humphrey et al., 1996) assuming simultaneous binding of both integrin motifs. Tal-F2/F3–integrin peptide complex (PDB ID 1MK7) was used as a starting model, and the docked α-helix (see previous section) was connected to the rest of the integrin sequence by manually building the missing residues 734–738. The protein complex was placed in a 98 × 71 × 73 Å box filled with 13,915 TIP3 explicit water models (overall system size 45,403 atoms) and subjected to energy minimization. Minimization and MD calculations were performed using the CHARMM27 (MacKerell et al., 1998) force field in the program NAMD (Nelson et al., 1996). Each minimization phase contained 4,000 steps and involved conjugate gradient and line search algorithms implemented in the NAMD package. In the first minimization phase, all of the protein atoms were fixed, and the water molecules were allowed to move. Then, both binding motifs of the integrin peptide were constrained by fixing all protein atoms except the inserted integrin residues 734–738. The third minimization phase was performed on all protein Cα atoms fixed to allow side chain optimization. Finally, all atoms were released in the fourth minimization step. Then, the system was gradually heated up to 310 K during 31-ps MD simulation using Berendsen barostat (1 atm; Berendsen et al., 1984). Constant temperature (310 K) and pressure (1 atm) MD simulation was then continued for 2–3 ns. Calculations were performed by using parallel processing with 64–256 processors.

## Western blotting and GST pull-down assays

SDS-PAGE and Western blotting of cellular lysates or precipitates were performed according to standard protocols. GST pull-down experiments were performed from lysates of COS-7 cells transiently transfected with EGFP-tagged wild-type or mutant β3-integrin for 48 h. Lysates were obtained after incubation with protease inhibitor containing radioimmunoprecipitation assay buffer on ice for 5 min and cleared by centrifugation and preadsorbed on uncoupled glutathione–Sepharose 4B beads (GE Healthcare). Concentrations of lysates were adjusted before the pull-down assay according to the expression levels of the different wild-type and mutant integrin constructs determined by Western blotting. Lysates were then incubated at 4°C on GST- or GST–Tal-H–loaded glutathione–Sepharose beads for 1 h. After washing in radioimmunoprecipitation assay buffer, beads were boiled, and proteins were separated on SDS-PAGE. ECFP-tagged Tal fragments or endogenous and mCherry-tagged FL-Tal proteins were revealed with mouse anti-EGFP mAb (clone B34; Covance) or anti-Tal mAb (clone 8D4; Sigma-Aldrich) followed by goat anti–mouse horseradish peroxidase–coupled secondary antibody (Jackson ImmunoResearch Laboratories, Inc.) and revealed by ECL (GE Healthcare).

## Online supplemental material

Fig. S1 shows the $Mn^{2+}$-induced integrin clustering on different substrates. Fig. S2 demonstrates the different localization pattern of FL, head, and rod domain fragments of mCherry-Tal with wild-type EGFP-tagged β3-integrin constructs after $Mn^{2+}$ induction of Tal-H–integrin clusters. Fig. S3 demonstrates the F-actin and vinculin distribution patterns in respect to $Mn^{2+}$-induced clustering of β3-integrins in cells coexpressing Tal-H or both Tal-H with Tal-R. Fig. S4 shows GST–Tal-H fusion proteins, SPR controls, and the expression of Tal-H mutants. Fig. S5 shows the phenotype and quantification of β3-integrin clustering in B16F1 melanoma cells transfected with wild-type or K364A mutant Tal-H in the absence of $Mn^{2+}$ and a comparison between wild-type and K364A mutant Tal–integrin associations performed by MD analysis. Online supplemental material is available at http://www.jcb.org/cgi/content/full/jcb.200908134/DC1.

# References

Anthis, N.J., K.L. Wegener, F. Ye, C. Kim, B.T. Goult, E.D. Lowe, I. Vakonakis, N. Bate, D.R. Critchley, M.H. Ginsberg, and I.D. Campbell. 2009. The structure of an integrin/talin complex reveals the basis of inside-out signal transduction. *EMBO J.* doi:10.1038/emboj.2009.287

Ballestrem, C., B. Hinz, B.A. Imhof, and B. Wehrle-Haller. 2001. Marching at the front and dragging behind: differential αVβ3-integrin turnover regulates focal adhesion behavior. *J. Cell Biol.* 155:1319–1332. doi:10.1083/jcb.200107107

Barret, C., C. Roy, P. Montcourrier, P. Mangeat, and V. Niggli. 2000. Mutagenesis of the phosphatidylinositol 4,5-bisphosphate (PIP$_2$) binding site in the NH$_2$-terminal domain of ezrin correlates with its altered cellular distribution. *J. Cell Biol.* 151:1067–1080. doi:10.1083/jcb.151.5.1067

Berendsen, H.J.C., J.P.M. Postma, W.F. Vangunsteren, A. Dinola, and J.R. Haak. 1984. Molecular dynamics with coupling to an external bath. *J. Chem. Phys.* 81:3684–3690. doi:10.1063/1.448118

Chabadel, A., I. Bañon-Rodríguez, D. Cluet, B.B. Rudkin, B. Wehrle-Haller, E. Genot, P. Jurdic, I.M. Anton, and F. Saltel. 2007. CD44 and beta3 integrin organize two functionally distinct actin-based domains in osteoclasts. *Mol. Biol. Cell.* 18:4899–4910. doi:10.1091/mbc.E07-04-0378

Cluzel, C., F. Saltel, J. Lussi, F. Paulhe, B.A. Imhof, and B. Wehrle-Haller. 2005. The mechanisms and dynamics of αvβ3 integrin clustering in living cells. *J. Cell Biol.* 171:383–392. doi:10.1083/jcb.200503017

Czuchra, A., H. Meyer, K.R. Legate, C. Brakebusch, and R. Fässler. 2006. Genetic analysis of β1 integrin "activation motifs" in mice. *J. Cell Biol.* 174:889–899. doi:10.1083/jcb.200604060

de Pereda, J.M., K.L. Wegener, E. Santelli, N. Bate, M.H. Ginsberg, D.R. Critchley, I.D. Campbell, and R.C. Liddington. 2005. Structural basis for phosphatidylinositol phosphate kinase type Igamma binding to talin at focal adhesions. *J. Biol. Chem.* 280:8381–8386. doi:10.1074/jbc.M413180200

del Rio, A., R. Perez-Jimenez, R. Liu, P. Roca-Cusachs, J.M. Fernandez, and M.P. Sheetz. 2009. Stretching single talin rod molecules activates vinculin binding. *Science.* 323:638–641. doi:10.1126/science.1162912

Dustin, M.L., and D.R. Colman. 2002. Neural and immunological synaptic relations. *Science.* 298:785–789. doi:10.1126/science.1076386

Eisenstein, M., I. Shariv, G. Koren, A.A. Friesem, and E. Katchalski-Katzir. 1997. Modeling supra-molecular helices: extension of the molecular surface recognition algorithm and application to the protein coat of the tobacco mosaic virus. *J. Mol. Biol.* 266:135–143. doi:10.1006/jmbi.1996.0773

Fievet, B.T., A. Gautreau, C. Roy, L. Del Maestro, P. Mangeat, D. Louvard, and M. Arpin. 2004. Phosphoinositide binding and phosphorylation act sequentially in the activation mechanism of ezrin. *J. Cell Biol.* 164:653–659. doi:10.1083/jcb.200307032

Franco, S.J., M.A. Senetar, W.T.N. Simonson, A. Huttenlocher, and R.O. McCann. 2006. The conserved C-terminal I/LWEQ module targets Talin1 to focal adhesions. *Cell Motil. Cytoskeleton.* 63:563–581. doi:10.1002/cm.20145

García-Alvarez, B., J.M. de Pereda, D.A. Calderwood, T.S. Ulmer, D. Critchley, I.D. Campbell, M.H. Ginsberg, and R.C. Liddington. 2003. Structural determinants of integrin recognition by talin. *Mol. Cell.* 11:49–58. doi:10.1016/S1097-2765(02)00823-7

Gaus, K., S. Le Lay, N. Balasubramanian, and M.A. Schwartz. 2006. Integrin-mediated adhesion regulates membrane order. *J. Cell Biol.* 174:725–734. doi:10.1083/jcb.200603034

Geiger, B., and A. Bershadsky. 2001. Assembly and mechanosensory function of focal contacts. *Curr. Opin. Cell Biol.* 13:584–592. doi:10.1016/S0955-0674(00)00255-6

Gingras, A.R., N. Bate, B.T. Goult, L. Hazelwood, I. Canestrelli, J.G. Grossmann, H. Liu, N.S. Putz, G.C. Roberts, N. Volkmann, et al. 2008. The structure of the C-terminal actin-binding domain of talin. *EMBO J.* 27:458–469. doi:10.1038/sj.emboj.7601965

Gingras, A.R., W.H. Ziegler, A.A. Bobkov, M.G. Joyce, D. Fasci, M. Himmel, S. Rothemund, A. Ritter, J.G. Grossmann, B. Patel, et al. 2009. Structural determinants of integrin binding to the talin rod. *J. Biol. Chem.* 284:8866–8876. doi:10.1074/jbc.M805937200

Goksoy, E., Y.Q. Ma, X. Wang, X. Kong, D. Perera, E.F. Plow, and J. Qin. 2008. Structural basis for the autoinhibition of talin in regulating integrin activation. *Mol. Cell.* 31:124–133. doi:10.1016/j.molcel.2008.06.011

Goult, B.T., N. Bate, N.J. Anthis, K.L. Wegener, A.R. Gingras, B. Patel, I.L. Barsukov, I.D. Campbell, G.C. Roberts, and D.R. Critchley. 2009. The structure of an interdomain complex that regulates talin activity. *J. Biol. Chem.* 284:15097–15106. doi:10.1074/jbc.M900078200

Hamada, K., T. Shimizu, T. Matsui, S. Tsukita, and T. Hakoshima. 2000. Structural basis of the membrane-targeting and unmasking mechanisms of the radixin FERM domain. *EMBO J.* 19:4449–4462. doi:10.1093/emboj/19.17.4449

Hughes, P.E., F. Diaz-Gonzalez, L. Leong, C. Wu, J.A. McDonald, S.J. Shattil, and M.H. Ginsberg. 1996. Breaking the integrin hinge. A defined structural constraint regulates integrin signaling. *J. Biol. Chem.* 271:6571–6574. doi:10.1074/jbc.271.12.6571

Humphrey, W., A. Dalke, and K. Schulten. 1996. VMD: visual molecular dynamics. *J. Mol. Graph.* 14:33–38: 27–28. doi:10.1016/0263-7855(96)00018-5

Hynes, R.O. 2002. Integrins: bidirectional, allosteric signaling machines. *Cell.* 110:673–687. doi:10.1016/S0092-8674(02)00971-6

Hytönen, V.P., and V. Vogel. 2008. How force might activate talin's vinculin binding sites: SMD reveals a structural mechanism. *PLOS Comput. Biol.* 4:e24. doi:10.1371/journal.pcbi.0040024

Kim, C., T.L. Lau, T.S. Ulmer, and M.H. Ginsberg. 2009. Interactions of platelet integrin alphaIIb and beta3 transmembrane domains in mammalian cell membranes and their role in integrin activation. *Blood.* 113:4747–4753. doi:10.1182/blood-2008-10-186551

Kim, M., C.V. Carman, and T.A. Springer. 2003. Bidirectional transmembrane signaling by cytoplasmic domain separation in integrins. *Science.* 301:1720–1725. doi:10.1126/science.1084174

Kim, M., C.V. Carman, W. Yang, A. Salas, and T.A. Springer. 2004. The primacy of affinity over clustering in regulation of adhesiveness of the integrin α$_L$β2. *J. Cell Biol.* 167:1241–1253. doi:10.1083/jcb.200404160

Lau, T.L., C. Kim, M.H. Ginsberg, and T.S. Ulmer. 2009. The structure of the integrin alphaIIbbeta3 transmembrane complex explains integrin transmembrane signalling. *EMBO J.* 28:1351–1361. doi:10.1038/emboj.2009.63

Legler, D.F., G. Wiedle, F.P. Ross, and B.A. Imhof. 2001. Superactivation of integrin alphavbeta3 by low antagonist concentrations. *J. Cell Sci.* 114:1545–1553.

Ma, Y.Q., J. Qin, C. Wu, and E.F. Plow. 2008. Kindlin-2 (Mig-2): a co-activator of β3 integrins. *J. Cell Biol.* 181:439–446. doi:10.1083/jcb.200710196

MacKerell, A.D., Jr., D. Bashford, M. Bellott, R.L. Dunbrack Jr., J.D. Evanseck, M.J. Field, S. Fischer, J. Gao, H. Guo, S. Ha, et al. 1998. All-atom empirical potential for molecular modeling and dynamics studies of proteins. *J. Phys. Chem. B.* 102:3586–3616. doi:10.1021/jp973084f

Martel, V., C. Racaud-Sultan, S. Dupe, C. Marie, F. Paulhe, A. Galmiche, M.R. Block, and C. Albiges-Rizo. 2001. Conformation, localization, and integrin binding of talin depend on its interaction with phosphoinositides. *J. Biol. Chem.* 276:21217–21227. doi:10.1074/jbc.M102373200

Miyamoto, S., S.K. Akiyama, and K.M. Yamada. 1995. Synergistic roles for receptor occupancy and aggregation in integrin transmembrane function. *Science.* 267:883–885. doi:10.1126/science.7846531

Mortier, E., G. Wuytens, I. Leenaerts, F. Hannes, M.Y. Heung, G. Degeest, G. David, and P. Zimmermann. 2005. Nuclear speckles and nucleoli targeting by PIP2-PDZ domain interactions. *EMBO J.* 24:2556–2565. doi:10.1038/sj.emboj.7600722

Moser, M., B. Nieswandt, S. Ussar, M. Pozgajova, and R. Fässler. 2008. Kindlin-3 is essential for integrin activation and platelet aggregation. *Nat. Med.* 14:325–330. doi:10.1038/nm1722

Nelson, M.T., W. Humphrey, A. Gursoy, A. Dalke, L.V. Kalé, R.D. Skeel, and K. Schulten. 1996. NAMD: a parallel, object oriented molecular dynamics program. *International Journal of High Performance Computing Applications.* 10:251–268. doi:10.1177/109434209601000401

Petrich, B.G., P. Fogelstrand, A.W. Partridge, N. Yousefi, A.J. Ablooglu, S.J. Shattil, and M.H. Ginsberg. 2007a. The antithrombotic potential of selective blockade of talin-dependent integrin alpha IIb beta 3 (platelet GPIIb-IIIa) activation. *J. Clin. Invest.* 117:2250–2259. doi:10.1172/JCI31024

Petrich, B.G., P. Marchese, Z.M. Ruggeri, S. Spiess, R.A. Weichert, F. Ye, R. Tiedt, R.C. Skoda, S.J. Monkley, D.R. Critchley, and M.H. Ginsberg. 2007b. Talin is required for integrin-mediated platelet function in hemostasis and thrombosis. *J. Exp. Med.* 204:3103–3111. doi:10.1084/jem.20071800

Rodius, S., O. Chaloin, M. Moes, E. Schaffner-Reckinger, I. Landrieu, G. Lippens, M. Lin, J. Zhang, and N. Kieffer. 2008. The talin rod IBS2 alpha-helix interacts with the beta3 integrin cytoplasmic tail membrane-proximal helix by establishing charge complementary salt bridges. *J. Biol. Chem.* 283:24212–24223. doi:10.1074/jbc.M709704200

Shaner, N.C., R.E. Campbell, P.A. Steinbach, B.N. Giepmans, A.E. Palmer, and R.Y. Tsien. 2004. Improved monomeric red, orange and yellow fluorescent proteins derived from *Discosoma* sp. red fluorescent protein. *Nat. Biotechnol.* 22:1567–1572. doi:10.1038/nbt1037

Tadokoro, S., S.J. Shattil, K. Eto, V. Tai, R.C. Liddington, J.M. de Pereda, M.H. Ginsberg, and D.A. Calderwood. 2003. Talin binding to integrin beta tails: a final common step in integrin activation. *Science*. 302:103–106. doi:10.1126/science.1086652

Takagi, J., B.M. Petre, T. Walz, and T.A. Springer. 2002. Global conformational rearrangements in integrin extracellular domains in outside-in and inside-out signaling. *Cell*. 110:599–11. doi:10.1016/S0092-8674(02)00935-2

Tanentzapf, G., and N.H. Brown. 2006. An interaction between integrin and the talin FERM domain mediates integrin activation but not linkage to the cytoskeleton. *Nat. Cell Biol.* 8:601–606. doi:10.1038/ncb1411

Vinogradova, O., J. Vaynberg, X. Kong, T.A. Haas, E.F. Plow, and J. Qin. 2004. Membrane-mediated structural transitions at the cytoplasmic face during integrin activation. *Proc. Natl. Acad. Sci. USA*. 101:4094–4099. doi:10.1073/pnas.0400742101

Vogel, V., and M.P. Sheetz. 2009. Cell fate regulation by coupling mechanical cycles to biochemical signaling pathways. *Curr. Opin. Cell Biol.* 21:38–46. doi:10.1016/j.ceb.2009.01.002

Wegener, K.L., A.W. Partridge, J. Han, A.R. Pickford, R.C. Liddington, M.H. Ginsberg, and I.D. Campbell. 2007. Structural basis of integrin activation by talin. *Cell*. 128:171–182. doi:10.1016/j.cell.2006.10.048

Wehrle-Haller, B., and B.A. Imhof. 2002. The inner lives of focal adhesions. *Trends Cell Biol.* 12:382–389. doi:10.1016/S0962-8924(02)02321-8

Xiao, T., J. Takagi, B.S. Coller, J.H. Wang, and T.A. Springer. 2004. Structural basis for allostery in integrins and binding to fibrinogen-mimetic therapeutics. *Nature*. 432:59–67. doi:10.1038/nature02976

Xiong, J.P., T. Stehle, B. Diefenbach, R. Zhang, R. Dunker, D.L. Scott, A. Joachimiak, S.L. Goodman, and M.A. Arnaout. 2001. Crystal structure of the extracellular segment of integrin alpha Vbeta3. *Science*. 294:339–345. doi:10.1126/science.1064535

Xiong, J.P., T. Stehle, R. Zhang, A. Joachimiak, M. Frech, S.L. Goodman, and M.A. Arnaout. 2002. Crystal structure of the extracellular segment of integrin alpha Vbeta3 in complex with an Arg-Gly-Asp ligand. *Science*. 296:151–155. doi:10.1126/science.1069040

Yan, B., D.A. Calderwood, B. Yaspan, and M.H. Ginsberg. 2001. Calpain cleavage promotes talin binding to the beta 3 integrin cytoplasmic domain. *J. Biol. Chem.* 276:28164–28170. doi:10.1074/jbc.M104161200

Zaidel-Bar, R., C. Ballestrem, Z. Kam, and B. Geiger. 2003. Early molecular events in the assembly of matrix adhesions at the leading edge of migrating cells. *J. Cell Sci.* 116:4605–4613. doi:10.1242/jcs.00792

Zhang, X., G. Jiang, Y. Cai, S.J. Monkley, D.R. Critchley, and M.P. Sheetz. 2008. Talin depletion reveals independence of initial cell spreading from integrin activation and traction. *Nat. Cell Biol.* 10:1062–1068. doi:10.1038/ncb1765

Zhu, J., B.H. Luo, P. Barth, J. Schonbrun, D. Baker, and T.A. Springer. 2009. The structure of a receptor with two associating transmembrane domains on the cell surface: integrin alphaIIbbeta3. *Mol. Cell*. 34:234–249. doi:10.1016/j.molcel.2009.02.022

Zimmermann, P., K. Meerschaert, G. Reekmans, I. Leenaerts, J.V. Small, J. Vandekerckhove, G. David, and J. Gettemans. 2002. PIP(2)-PDZ domain binding controls the association of syntenin with the plasma membrane. *Mol. Cell*. 9:1215–1225. doi:10.1016/S1097-2765(02)00549-X